DOI: 10.1002/adma.200702242

Developments in Nanostructured Cathode Materials for High-Performance Lithium-Ion Batteries**

*Ying Wang** and *Guozhong Cao**

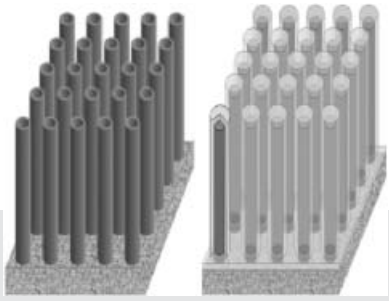

Nanostructured materials lie at the heart of fundamental advances in efficient energy storage and/or conversion, in which surface processes and transport kinetics play determining roles. This Review describes some recent developments in the synthesis and characterization of nanostructured cathode materials, including lithium transition metal oxides, vanadium oxides, manganese oxides, lithium phosphates, and various nanostructured composites. The major goal of this Review is to highlight some new progress in using these nanostructured materials as cathodes to develop lithium batteries with high energy density, high rate capability, and excellent cycling stability resulting from their huge surface area, short distance for mass and charge transport, and freedom for volume change in nanostructured materials.

1. Introduction

1.1. General Background

Recent increases in demand for oil, associated price increases, and environmental issues are continuing to exert pressure on an already stretched world energy infrastructure. Significant progress has been made in the development of renewable energy technologies such as solar cells, fuel cells, and biofuels. In the past, these types of energy sources have been marginalized, but as new technology makes alternative energy more practical and price competitive with fossil fuels, it is expected that the coming decades will usher in a long-expected transition away from oil and gasoline as our primary fuel. Although a variety of renewable energy technologies have been developed, they have not reached wide-spread use. High performance of such technologies is mainly achieved through designed sophisticated device structures with multiple materials, for example tandem cells in photovoltaic devices. Almost all of the alternative energy technologies are limited by the materials properties. For example, poor charge carrier mobilities in organic/polymer semiconductors limit the energy conversion efficiency of organic photovoltaic cells to less than 6%. Thermoelectrics typically possess an energy conversion efficiency of less than 3%. Portable electric power sources have lower energy and power density largely resulting from poor charge and mass transport properties. New materials that are chemically modified through molecular or atomic engineering and/or possess unique microstructures would offer significantly enhanced properties for more efficient energy conversion devices and high-density energy/power storage.

[*] Y. Wang,[+] G. Cao
Department of Materials Science and Engineering
University of Washington
Seattle, WA 98195 (USA)
E-mail: ying-wang@northwestern.edu; gzcao@u.washington.edu

[+] Current address: Materials Research Institute and Department of Materials Science and Engineering, Northwestern University, Evanston, IL 60208, USA

[**] This work has been supported in part by the National Science Foundation (DMI-0455994) and the Air Force Office of Scientific Research (AFOSR-MURI, FA9550-06-1-032). This work has also been supported by the Center for Nanotechnology at UW, Pacific Northwest National Laboratories (PNNL), the Joint Institute of Nanoscience and Nanotechnology (JIN, UW, and PNNL), Washington Technology Center (WTC), and JFE Steel Corporation, Japan. Y.W. would like to acknowledge Ford, Nanotechnology, and JIN graduate fellowships. A portion of the research (TEM study) described in this paper was performed in the Environmental Molecular Sciences Laboratory, a national scientific user facility sponsored by the Department of Energy's Office of Biological and Environmental Research and located at PNNL.

One alternative energy/power source under serious consideration is electrochemical energy production, as long as this energy consumption is designed to be more sustainable and more environmentally benign. The lithium-ion battery is a representative system for such electrochemical energy storage and conversion. At present, lithium-ion batteries are efficient, light-weight, and rechargeable power sources for consumer electronics such as laptop computers, digital cameras, and cellular phones.[1] Moreover, they have been intensively studied for use as power supplies of electric vehicles (EVs) and hybrid electric vehicles (HEVs), which require high energy and power densities Lithium-ion batteries are attractive power-storage devices owning to their high energy density;[2] however, their power density is relatively low because of a large polarization at high charge–discharge rates. This polarization is caused by slow lithium diffusion in the active material and increases in the resistance of the electrolyte when the charging–discharging rate is increased. To overcome these problems, it is important to design and fabricate nanostructured electrode materials that provide high surface area and short diffusion paths for ionic transport and electronic conduction.

Nanomaterials offer unusual mechanical, electrical, and optical properties endowed by confining the dimensions of such materials, and the overall behaviors of nanomaterials exhibit combinations of bulk and surface properties.[3] Thus, nanostructured materials are drawing a tremendous amount of attention because of their novel properties, and because of their potential applications in a variety of nanodevices, such as field-effect transistors (FETs),[4–7] chemical and biological sensors,[8–11] nanoprobes,[12] and nanocables.[13] Reports on the processing, properties, and applications of nanomaterials are appear rapidly, on a daily basis. Many synthesis methods have been reported for the synthesis of nanostructured electrode materials. Among them, solution-based methods are well-known for their advantages in tailoring the size and morphology of the nanostructures. It is the uncomplicated sol–gel processing (soft chemistry) method in combination with template synthesis or hydrothermal treatment that produces the most desirable nanostructures with remarkable reliability, efficiency, selectivity, and variety. Template synthesis is a general method for preparing ordered arrays of nanostructures with nanorods/nanotubes/nanocables protruding from the underlying current collector.[14] Hydrothermal synthesis is another powerful tool to transform transition metal oxides into high-quality nanostructures. Other fabrication methods of nanostructures include the reverse micelle technique, and the size of nanostructures can be tuned easily by keeping the freshly made nanorods in the micellar solution.[15] This Review aims to give a concise and useful survey of recent progress on synthesis and characterizations of nanostructured cathode materials for lithium-ion batteries, starting with a brief overview on lithium-ion batteries and cathode materials as follows. It is clear that nanostructured cathode electrodes offer improved energy storage capacity and charge–discharge kinetics, as well as better cyclic stabilities, owing to their huge surface area for Faradaic reaction, short distance for mass and charge diffusion, as well as the added freedom for volume change that accompanies lithium-ion intercalation and discharge. However, nanostructured electrodes also introduce new challenges, as their huge surface area and nanometer size will unquestionably increase their solubility in electrolyte solutions.

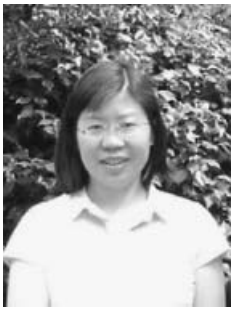

Ying Wang is currently a post-doctoral fellow under the supervision of Professor Robert P. H. Chang at the Materials Research Institute and Department of Materials Science and Engineering at Northwestern University. She received her Ph.D. in Materials Science and Engineering from the University of Washington (USA) in 2006, M.A. in Chemistry from Harvard University (USA) in 1999, and B.S. in Chemical Physics from the University of Science and Technology of China (P.R. China) in 1997. Her research interests include rechargeable batteries, solar cells, electrochromic displays, nanostructured materials, thin films, intercalation compounds, functional oxides, sol–gel processing, atomic layer deposition, and chemical vapor deposition. Her recent awards include the Nanotechnology Graduate Research Award from the University of Washington Initiative Fund (UIF, 2005), a Graduate Fellowship from the PNNL-UW Joint Institute for Nanoscience (JIN, 2005), and a Ford Motor Company Fellowship (2004). She has published about 20 journal papers and authored 4 book chapters.

Guozhong Cao is Professor of Materials Science and Engineering and Adjunct Professor of Chemical and Mechanical Engineering at the University of Washington. He received his Ph.D. from Eindhoven University of Technology (The Netherlands), M.S. from the Shanghai Institute of Ceramics (P.R. China), and B.S. from East China University of Science and Technology (P.R. China). Prior to joining the UW faculty in 1996, Dr. Cao worked briefly at the University of Twente and the University of Nijmegen (The Netherlands) and the Advanced Materials Lab, University of New Mexico and Sandia National Laboratories (USA). His major awards include a European Union Fellowship in 1993, a college Outstanding Educator Award in 1999, and a university Distinguished Teaching Award in 2000. He has published over 200 research papers, and authored and edited 4 books and 3 conference proceedings on nanotechnology. Currently, he serves as associate editor of the Journal of Nanophotonics. His current research is focused mainly on nanomaterials for energy conversion and storage.

ADVANCED MATERIALS

1.2. Lithium Batteries and Cathode Materials

A battery consists of three basic components: an anode, a cathode, and an electrolyte; and is a device that converts chemical potential to electric energy through Faradaic reactions, which includes heterogeneous charge transfer occurring at the surface of an electrode.[16] Batteries are broadly grouped as primary and secondary batteries. Primary batteries are single-use devices and can not be recharged; secondary batteries are also called rechargeable batteries and can be recharged for many times. In a typical secondary battery, energy storage involves Faradaic reactions occurring at the surface of an electrode, and mass and charge transfer through the electrode; therefore, the surface area and the transport distance play important roles in determining the performance of the battery in question. Chemical composition, crystal structure, and microstructure will have significant impacts on the surface reaction and transfer processes as well as on cyclic stability.

Intercalation electrodes in batteries are electroactive materials and serve as a host solid into which guest species are reversibly intercalated from an electrolyte. Intercalation compounds are a special family of materials. Intercalation refers to the reversible intercalation of mobile guest species (atoms, molecules, or ions) into a crystalline host lattice that contains an interconnected system of empty lattice sites of appropriate size, while the structural integrity of the host lattice is formally conserved.[17] The intercalation reactions typically occur around room temperature. A variety of host lattice structures have been found to undergo such low-temperature reactions.[18] However, intercalation reactions involving layered host lattices have been most extensively studied, partly owing to their structural flexibility and the ability to adapt to the geometry of the intercalated guest species by free adjustment of the interlayer separation. The readers are referred to a comprehensive and excellent article on inorganic intercalation compounds.[17] Despite the differences in chemical composition and lattice structure of the host sheets, all the layer hosts are characterized by strong interlayer covalent bonding and weak interlayer intercalations. The weak interlayer intercalations include van der Waals force or electrostatic attraction through oppositely charged species between two layers. Various host lattices are metal dichalcogenides, metal oxyhalides, metal phosphorous trisulphides, metal oxides, metal phosphates, hydrogen phosphates and phosphonates, graphite, and layered clay minerals. Guest materials include metal ions, organic molecules, and organometallic molecules. When guest species are incorporated into host lattices, various structural changes will take place. The fundamental geometrical transitions of layered host lattice matrices upon intercalation of guest species include: (1) change in interlayer spacing, (2) change in stacking mode of the layers, and (3) formation of intermediate phases at low guest concentrations.[19] There are various synthesis methods for the formation of intercalation compounds.[17,20] The most commonly used and simplest method is direct reaction of the guest species with the host lattice.[21] For direct reactions, the intercalation reagent must be a good reducing agent of the host crystals. Ion exchange is a method to replace the guest ion in an intercalation compound with another guest ion, which offers a useful route for intercalating large ions that do not intercalate directly.[22] Appropriate chosen solvents or electrolytes may assist the ion-exchange reactions by flocculating and reflocculating the host structure.[23] Electrointercalation is yet another method, in which the host lattice serves as the cathode of an electrochemical cell.[24] Electrochemical lithium intercalation occurs together with compensating electrons, leading to the formation of vanadium bronzes as follows:

$$V_2O_5 + xLi^+ + xe^- \leftrightarrow Li_xV_2O_5 \quad (1)$$

The principal concept of lithium-ion batteries is illustrated in Figure 1. A combination of a negative lithium intercalation material (anode) with another lithium intercalation material (cathode) having a more positive redox potential gives a Li-ion transfer cell. Anode and cathode are separated by the electrolyte, which is an electronic insulator but a Li-ion conductor. Upon charging, lithium ions are released by the cathode and intercalated at the anode. When the cell is discharged, lithium ions are extracted by the cathode and inserted into the anode. Early batteries used metallic lithium as anode, which combines a very negative redox potential with a low equivalent weight. It was later replaced by carbon because of safety concerns. Replacement of metallic lithium or carbon by lithium intercalation compounds improves both cell life and safety but at the expense of cell voltage, specific charge, and rate capability. Electrode materials must fulfill three fundamental requirements to reach the goal of a high specific energy and energy density: (1) a high specific charge and charge density, that is, a high number of available charge carriers per mass and volume unit of the material; (2) a high cell voltage, resulting from a high (cathode) and low (anode) standard redox potential of the respective electrode redox reaction; and (3) a high reversibility of electrochemical reactions at both cathodes and anodes to maintain the specific charge for hundreds of charge–discharge cycles.

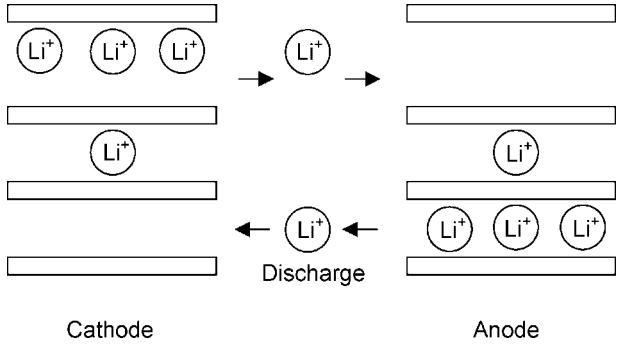

Figure 1. Schematic illustration of a lithium-ion battery.

Ever since the idea of a rechargeable lithium cell based on Li intercalation reactions was initiated in the early 1970s, numerous lithium intercalation electrodes have been proposed to date. The area of cathodes is much less developed than anodes,[25] and we will focus on the cathode materials in this article. Details on lithium-ion battery cathode materials can be found in recent reviews by Whittingham et al.[26,27] There are two categories of cathode materials. One comprises layered compounds with an anion close-packed lattice; transition metal cations occupy alternate layers between the anion sheets, and lithium ions are intercalated into remaining empty layers. $LiTiS_2$, $LiCoO_2$, $LiNi_{1-x}Co_xO_2$, and $LiNi_xMn_xCo_{1-2x}O_2$ all belong to this group. The spinels with transition metal cations ordered in all the layers can be considered to be in this group as well. This class of materials has the inherent advantage of higher energy density (energy per unit of volume) owning to their more compact lattices. The other group of cathode materials has more open structures, such as vanadium oxides, the tunnel compounds of manganese oxides, and transition metal phosphates (e.g., the olivine $LiFePO_4$). These materials generally provide the advantages of better safety and lower cost compared to the first group. Nanostructures offer huge surface area, short mass and charge diffusion distance, and freedom for volume change during charge–discharge cycles, and thus are expected to improve the lithium-ion intercalation properties. Quite some research has been reported in the literature, and more efforts are underway in many research groups. A comprehensive review to cover a large variety of nanostructured cathode materials to date would be necessary. This Review article is intended to fill this need through summarizing the recent progress in the synthesis and characterization of nanostructured cathode materials for efficient lithium ion intercalation and highlighting the important accomplishments and remaining challenges. Section 2 covers nanostructured lithium transition metal oxides and Section 3 reviews nanostructured vanadium oxides and nanostructured manganese oxides. In each section, we look firstly at structural and electrochemical properties of the materials, then at synthesis and characterization of nanostructures of these materials, that is, how synthesis methods and parameters affect properties, and how to improve electrochemical performance. The last point leads to a summary of various nanosized coatings on cathode materials in Section 4 and an overview on nanostructured composites in Section 5.

2. Nanostructured Lithium Transition Metal Oxides

Currently there are three intercalation materials that are used commercially as cathode materials for rechargeable lithium batteries: $LiCoO_2$, $LiNiO_2$, and $LiMn_2O_4$. $LiCoO_2$ is the most popular among the possible cathode materials owing to the convenience and simplicity of preparation. This material can be easily synthesized using both solid-state and chemical approaches.[28,29] The Li_xCoO_2 system has been studied extensively thus far.[30,31] Li_xCoO_2 exhibits excellent cyclability at room temperature for $1 > x > 0.5$. Therefore, the specific capacity of the material is limited to the range of 137 to 140 mA h g^{-1}, although the theoretical capacity of $LiCoO_2$ is 273 mA h g^{-1}.[32] On the other hand, Li_xCoO_2 is very expensive and highly toxic, which is unfortunate considering its good electrochemical properties and easy synthesis. The reversible capacity of Li_xNiO_2 is higher than that of Li_xCoO_2, since the amount of lithium that can be extracted/intercalated during redox cycles is around 0.55, in comparison with 0.5 for $LiCoO_2$, allowing the specific capacity to be more than 150 mA h g^{-1} with appropriate cyclability.[33] Although $LiNiO_2$ is isostructural to $LiCoO_2$, preparation of $LiNiO_2$ is more complicated. Because there are additional nickel ions on the lithium sites, and vice versa in the crystal structure of $LiNiO_2$, the Li–Ni–O system is represented by $Li_{1-y}Ni_{1+y}O_2$ with a deviation from the normal stoichiometry.[34,35] This special structure makes it very difficult to synthesize the stoichiometric oxide with all the lithium sites completely filled by lithium. $LiMn_2O_4$ is the third-most-popular cathode material for lithium-ion batteries. In comparison with $LiCoO_2$ and $LiNiO_2$, $LiMn_2O_4$ possesses essential advantages of less toxicity and having an abundant materials source. In principle, $Li_xMn_2O_4$ permits the intercalation/extraction of lithium ions in the range of $0 < x < 2$.[36] For intermediate values of x between 1 and 2 the material consists of two different phases: cubic in bulk and tetragonal at the surface. Simultaneously the intercalation of lithium ions effectively decreases the average valence of manganese ions and leads to a pronounced cooperative Jahn–Teller effect, in which the cubic spinel crystal becomes distorted tetragonal with a $c/a \approx 1.16$, and the volume of the unit cell increases by 6.5%. This high c/a ratio causes a low capacity, restricted to 120–125 mA h g^{-1}, and significant capacity degradation at moderate temperatures in the range of 50 to 70 °C.[37] To enhance the poor rate capability of lithium metal oxides often owning to the structural instability of some lithium metal oxides such as $LiNiO_2$ or $LiMnO_2$, light substitutions or preparing solid solutions of several lithium metal oxides have been explored and the new compounds have shown promising electrochemical characteristics.[38] However, lithium metal oxides still suffer from some intrinsic limitations. For example, $LiCoO_2$ has a decent lithium diffusion coefficient, 5×10^{-9} cm^2 s^{-1},[39] whereas the conductivity of this material is as low as 10^{-3} S cm^{-1}.[40] To improve the intercalation–deintercalation kinetics of the material, it is necessary to downsize the material to achieve short diffusion distance and large surface area.

There have been several recent reports on the synthesis and electrochemical properties of nanostructured lithium metal oxides. Heating the nanorodlike $LiNi_{0.5}Mn_{1.5}O_4$ up to 800 °C breaks the nanorods into nanoparticulate $LiNi_{0.5}Mn_{1.5}O_4$, with particle sizes in the range of 70–80 nm. Such a nanoparticulate $LiNi_{0.5}Mn_{1.5}O_4$ cathode shows good electrochemical characteristics at a wide range of rates (from C/4 to 15 C) when cycled between 3.5 and 5 V.

ADVANCED MATERIALS

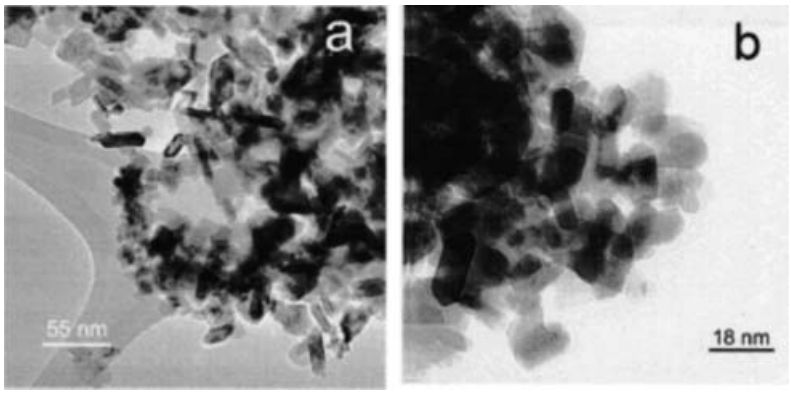

Figure 2. TEM images of $LiMn_2O_4$ spinels annealed at a) 350 °C and b) 450 °C. Adapted with permission from [41]. Copyright 2004 The Electrochemical Society.

As for the spinel $LiMn_2O_4$, synthesis of $LiMn_2O_4$ nanoparticles can be carried out by a sol–gel method combined with post-calcination, and the particle size is affected by the calcination temperature.[41] The nanoparticles have a size of 10 nm at a low temperature of 350 °C, whereas sub-micrometer-sized particles are obtained at a high temperature of 550 °C, as shown in the transmission electron microscopy (TEM) images (Fig. 2a and b). The $LiMn_2O_4$ nanoparticles were found to behave differently in different voltage ranges. In comparison with a large nonporous cathode, the nanoparticle cathode shows improved capacity and cycleability in the 3 V discharge range, while in the 4 V discharge region it exhibits decreased capacity and improved cycleability. The enhancement in capacity and cycleability is due to the reduced charge-transfer resistance of nanoparticulate cathode in comparison with a ''large'' cathode material.

A thin film of $LiCoO_2$ could be deposited at room temperature in a nanocrystalline state using planar magnetron radio-frequency (rf) sputtering.[42] Subsequent heating of the films at 300 °C causes the average grain size to increase but still within the nanosized dimensions, while the lattice distortion is reduced by the heating. Such nanocrystalline films of $LiCoO_2$ annealed at low temperature demonstrate improved electrochemical performance.

Nanostructured solid solutions of lithium metal oxides such as $LiNi_{0.5}Mn_{1.5}O_4$ can be synthesized using solution methods as well. A modified Pechini method has been employed to obtain nanostructured $LiNi_{0.5}Mn_{1.5}O_4$ by adding aqueous solutions of $Li(NO_3)$, $Mn(NO_3)_2 \cdot 4H_2O$, and $Ni(NO_3)_2 \cdot 6H_2O$ into a mixture of citric acid and ethylene glycol.[43] The as-prepared samples were sintered at different temperatures and resulted in ordered $P4_332$ (P) spinel or disordered $Fd3m$ (F) spinel. The disordered spinel contains a small amount of Mn^{3+} and has a higher electronic conductivity than the ordered sample, by two orders of magnitude. Therefore, the disordered spinel shows a higher rate capability than the ordered sample and exhibits a capacity retention of 80% at 6 C. Furthermore, the shape of nanostructured $LiNi_{0.5}Mn_{1.5}O_4$ can be tailored by a polymer-assisted method.[44] First, nanocrystalline oxalates were obtained by grinding hydrated salts and oxalic acid in the presence of polytheyleneglycol 400. Then, nanorodlike $LiNi_{0.5}Mn_{1.5}O_4$ was prepared by thermal decomposition of mixed nanocrystalline oxalates at 400 °C.

3. Nanostructured Metal Oxides

3.1. Nanostructured Vanadium Oxides

Vanadium oxide is a typical intercalation compound as a result of its layered structure. For Li-ion intercalation applications, vanadium oxide offers the essential advantages of low cost, an abundant source, easy synthesis, and high energy densities. Orthorhombic crystalline V_2O_5 consists of layers of VO_5 square pyramids that share edges and corners.[45,46] The reversible electrochemical lithium intercalation into V_2O_5 at room temperature was first reported by Whittingham in 1975.[47] In addition to crystalline V_2O_5, high Li intercalation capacity has been reported for hydrated vanadium pentoxides ($V_2O_5 \cdot nH_2O$), such as $V_2O_5 \cdot nH_2O$ glasses with P_2O_5 or other network formers,[48] $V_2O_5 \cdot nH_2O$ xerogels,[49,50] and $V_2O_5 \cdot nH_2O$ aerogels.[51] Specific energies of over 700 W A h kg^{-1} were measured for lithium cells with a xerogel cathode.[50] $V_2O_5 \cdot nH_2O$ xerogels are composed of ribbonlike particles and display lamellar ordering, with water molecules intercalated between the layers.[52] These water molecules expand the distance between the layers, and the intercalation capacities of $V_2O_5 \cdot nH_2O$ xerogels are enhanced as a result.[50] The structure of the $V_2O_5 \cdot nH_2O$ xerogel can be illustrated as an assembly of well-defined bilayers of single V_2O_5 layers made of square pyramidal VO_5 units with water molecules residing between them.[52] This structure possesses enough atomic ordering to perhaps be characterized as nanocrystalline.

To date there are a large number of publications on nanostructures of vanadium oxides. Pioneering work on the synthesis and electrochemical properties of vanadium oxide nanorolls was carried out by Spahr et al.[53] In their synthesis, a combination of sol–gel reaction and hydrothermal treatment of vanadium oxide precursor is conducted in the presence of an amine that acts as structure-directing template.[53,54–57] The resultant nanoroll is either constructed in closed concentric cylinders (nanotubes) or formed by scrolling one or more layers (nanoscrolls). If amine is replaced by ammonia during the hydrolysis step, a new type of vanadium oxide nanoroll (nanotube) with alternating interlayer distances is obtained.[58] Such a unique structure is first observed in a tubular phase. Compared to other tubular systems, the vanadium oxide nanorolls are especially interesting because they possess four different contact regions, that is, tube opening, outer surface, inner surface, and interstitial region. VO_x nanorolls can intercalate a variety of molecules and ions reversibly without change in the crystalline structure. The Li intercalation capacities have been found up to 200 mA h g^{-1}, however, there is structural breakdown during redox cycles and

degradation in cycling performance owing to the morphological flexibility. The cyclic voltammetry measurements show that the well-ordered nanorolls behave closely to classic crystalline vanadium pentoxide, while the defect-rich nanorolls have electrochemical behavior similar to that of sol–gel-prepared hydrated vanadium pentoxide materials. The specific capacity of defect-rich nanorolls (340 mA h g^{-1}) is higher than that of the well-ordered nanorolls (240 mA h g^{-1}) under comparable conditions.

Martin and co-workers have reported a series of studies on polycrystalline V_2O_5 nanorod arrays. They used a template-based method by depositing triisopropoxyvanadium(V) oxide (TIVO) into the pores of polycarbonate filtration membranes followed by removal of membranes at high temperature.[59] The V_2O_5 nanorod arrays deliver three times the capacity of the thin-film electrode at a high rate of 200°C and four times the capacity of the thin-film control electrode above 500°C. After that, Li and Martin achieved improved volumetric energy densities of V_2O_5 nanorod arrays by chemically etching the polycarbonate membrane to increase its porosity prior to template synthesis.[60] In the latest work of Sides and Martin, V_2O_5 nanorods of different diameters were prepared and their electrochemical properties at low temperature were compared.[61] V_2O_5 nanorods with nanometer-sized diameters (e.g., 70 nm) deliver dramatically higher specific discharge capacities at low temperature than V_2O_5 nanorods with micrometer-sized diameters. Thus, Li-ion battery electrodes composed of nanosized materials meet the low-temperature performance challenge, because nanomaterials palliate the problems of slow electrochemical kinetics and the slow diffusion by offering high surface area and short diffusion distance.

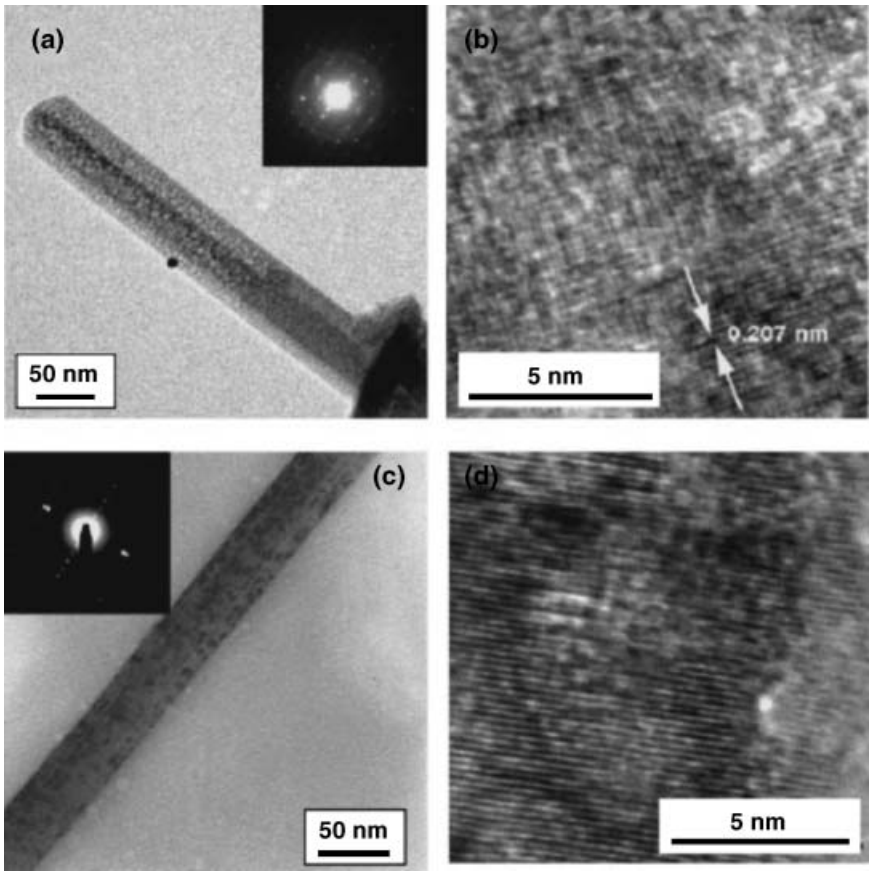

Figure 3. a) TEM image and selected-area electron diffraction pattern of a V_2O_5 nanorod prepared from template-based electrochemical deposition from $VOSO_4$ solution. b) High-resolution TEM image of the V_2O_5 nanorod in (a), showing lattice fringes. The spacing of the fringes was measured to be 0.207 nm. c) TEM image and selected area electron diffraction pattern of a V_2O_5 nanorod prepared from template-based electrophoretic deposition from V_2O_5 sol. d) High-resolution TEM image of the V_2O_5 nanorod in (c). The spacing of the fringes was measured to be 0.208 nm. The nanorods grown from both routes were demonstrated to have a single-crystalline nature or, at least, a well-textured nature of the grown nanorods with a [010] growth direction. Adapted with permission from [63]. Copyright 2005 The Institute of Pure and Applied Physics.

Synthesis and electrochemical properties of single-crystal V_2O_5 nanorod arrays were first reported by Cao's group.[62–64] They utilized a template-based electrodeposition method by depositing V_2O_5 into pores of polycarbonate templates with the assistance of electric field from three different types of solutions or sol, that is, VO^{2+} solution, VO_2^+ solution, and V_2O_5 sol. Figure 3a and c shows TEM images of a V_2O_5 nanorod and selected-area electron diffraction patterns, which clearly demonstrate the single-crystalline nature or, at least, well-textured nature of the grown nanorods with a [010] growth direction for nanorods grown from both routes. Figure 3b and d also shows high-resolution TEM images of a single V_2O_5 nanorod, in which lattice fringes are clearly visible. The spacing of the fringes was measured to be 0.207 nm for nanorod grown from route A, and 0.208 nm for nanorods obtained from V_2O_5 sol. These values are similar for different synthesis route and correspond well with the spacing of (202) planes at 0.204 nm. These fringes make an angle of 88.9° with the long axis of the nanorod, which is consistent with a growth direction of [010]. Similar measurements made on high-resolution images of other nanorods also yield results consistent with a [010] growth direction. The formation of single-crystal nanorods from solutions by electrochemical deposition is attributed to evolution selection growth (Fig. 4a). The initial heterogeneous nucleation or deposition on the substrate surface results in the formation of nuclei with random orientation. The subsequent growth of various facets of a nucleus is dependent on the surface energy, and varies significantly from one facet to

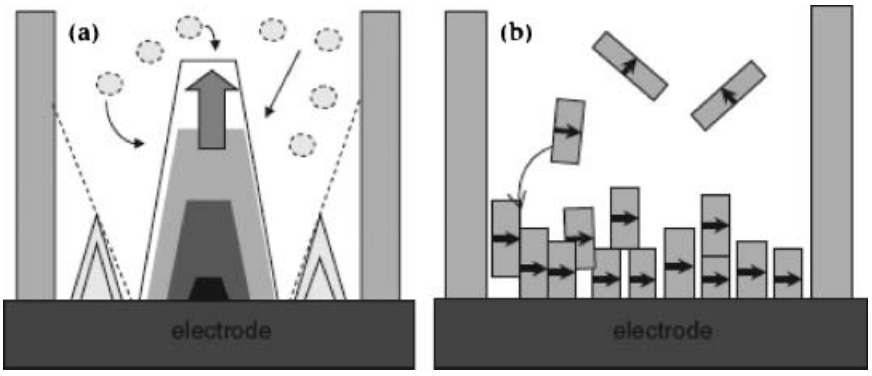

Figure 4. Schematic illustrations of growth mechanisms of single crystalline nanorods: a) evolution selection growth, and b) homoepitaxial aggregation. Adapted with permission from [63]. Copyright 2005 The Institute of Pure and Applied Physics.

another.[65] In the case of nanorods made from the V_2O_5 sol by electrophoretic deposition, the formation of single-crystal nanorods is explained by homoepitaxial aggregation of crystalline nanoparticles (Fig. 4b). Thermodynamically it is favorable for the crystalline nanoparticles to aggregate epitaxially; such growth behavior and mechanism have been well reported in literature.[66,67] As a result, V_2O_5 nanorods grown by electrochemical deposition from solutions are dense single crystals, while the nanorods grown from sol electrophoresis are also single-crystalline but have many defects inside the crystal. Such difference in nanostructure determines the different electrochemical behavior of nanorods grown from different solutions or sol. The nanorods grown from V_2O_5 sol by electrophoresis show the best kinetic properties for Li-ion intercalation. All the V_2O_5 nanorod arrays show higher capacity and enhanced rate capability in comparison with the sol–gel derived polycrystalline V_2O_5 film. For example, the V_2O_5 nanorod arrays grown from VO^{2+} solution deliver five times the capacity of the film at a current density of $0.7\,A\,g^{-1}$. For the single-crystal nanorod arrays, the long axis (growth direction) is parallel to the interlayers of V_2O_5, thus, the nanorods provide shorter and simpler diffusion paths for lithium ions and allow the most freedom for dimension change. Using the similar template-based electrodeposition method but with different growth conditions, Wang et al. prepared nanotube arrays of $V_2O_5{\cdot}nH_2O$.[68] The authors found that nanotubes resulted when using lower voltages and shorter deposition times compared to the conditions for preparing nanorods. The $V_2O_5{\cdot}nH_2O$ nanotube arrays demonstrate an initial high capacity of $300\,mA\,h\,g^{-1}$, about twice the initial capacity of $140\,mA\,h\,g^{-1}$ from the $V_2O_5{\cdot}nH_2O$ film. Such enhancement of capacity is due to the large surface area and short diffusion distances offered by the nanotube array. Subsequently, the authors used a two-step electrodeposition method to prepare Ni–$V_2O_5{\cdot}nH_2O$ core/shell nanocable arrays.[69] Ni nanorod arrays were first grown by the template-based electrochemical deposition. In the second step, the hydrated vanadium pentoxide shell was deposited onto the surface of nickel nanorods through sol electrophoretic deposition. Figure 5 compares the electrochemical performance of Ni–$V_2O_5{\cdot}nH_2O$ nanocable arrays, single-crystal V_2O_5 nanorod arrays and sol–gel-derived V_2O_5 films. Obviously Ni–$V_2O_5{\cdot}nH_2O$ nanocable arrays demonstrate remarkably improved capacity and rate capability in comparison with the other two. The intercalation capacities of both nanorod arrays and sol–gel films decrease rapidly as the current density increases, while nanocable arrays are able to retain the high capacity at high current density (discharge rate), indicating the excellent high-rate performance of nanocable arrays. As shown in Figure 5c, Ni–$V_2O_5{\cdot}nH_2O$ nanocable array has significantly higher energy density and power density than those of the nanorod array and sol–gel film by at least one order of magnitude, which is ascribed to the enhanced surface area and the reduced internal resistance.

Following the systematic studies on ordered arrays of V_2O_5 nanorods, nanotubes, and nanocables, Lee and Cao reported the synthesis and electrochemical properties of V_2O_5 films with nanosized features.[70] Typically, platelet- and fibrillar-structured V_2O_5 films were prepared by solution methods, and the discharge capacities and cyclic performance of these films were compared with those of the conventional plain structured film. The platelet film consists of 20–30 nm sized standing platelets perpendicular to the substrate with random orientation, whereas fibrillar film is comprised of randomly oriented fibers though most of them protrude from the substrate surface. The initial discharge capacities of platelet and fibrillar structured V_2O_5 films are 1240 and $720\,mA\,h\,g^{-1}$, respectively, which are far larger than the initial discharge value ($260\,mA\,h\,g^{-1}$) of the plain-structure film. Such large discharge capacity values are ascribed to the combined effects of the reduced Li^+ diffusion distance, which prevents concentration polarization of Li^+ in the V_2O_5 electrode and poor interlayered cross-linking offering more Li^+ intercalation. However, platelet- and fibrillar-structured V_2O_5 films were easily degraded during electrochemical cyclic tests. Similarly platelet-structured V_2O_5 films are also obtained by dc sputtering, but show good cycling performance.[71] The capacity only changes from 80 to $73\,\mu A\,h\,cm^{-2}$ after 100 cycles and to $70\,\mu A\,h\,cm^{-2}$ after 200 cycles at a current density of $100\,\mu A\,cm^{-2}$. These results can be explained by the *h*00 preferred orientation of the film, which ensures a good homogeneity for Li intercalation–deintercalation and thus a good cycleability.

In addition to V_2O_5 thin films with structural features on the nanoscale, three-dimensional ordered macroporous (3DOM) V_2O_5 electrode materials with nanometer-sized features were synthesized using a colloidal-crystal-templated method.[72] The method is based on soaking the poly(methyl methacrylate) (PMMA) colloidal crystals in the $NaVO_3$ solution so that the interstitial spaces are infiltrated with precursor solution,

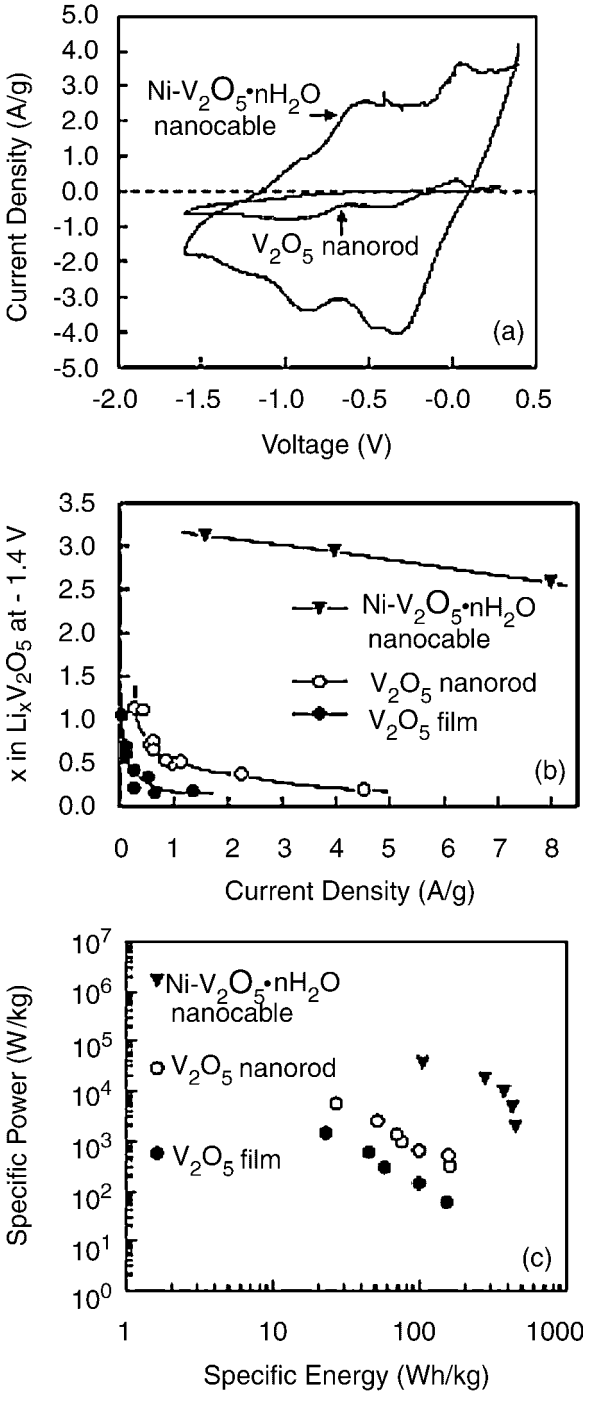

Figure 5. a) Cyclic voltammograms of Ni-$V_2O_5 \cdot n H_2O$ nanocable array and V_2O_5 nanorod array using a scan rate of $10\,mV\,s^{-1}$. b) Relationship between current density and Li intercalation capacity of Ni-$V_2O_5 \cdot n H_2O$ nanocable array, V_2O_5 nanorod array and sol-gel film from chronopotentiometric measurements. c) Ragone plot for Ni-$V_2O_5 \cdot n H_2O$ nanocable array, V_2O_5 nanorod array and sol-gel film. Adapted with permission from [69]. Copyright 2005 American Chemical Society.

followed by chemical conversion, drying, and sintering to remove polymer spheres. The resultant material possesses photonic-crystal structures composed of interconnected open pores with nanometer-sized thin walls. Such three-dimensional ordered structure provide several advantageous features for the Li-ion intercalation–deintercalation process: the continuous network ensures the electrical conductivity, the large open pores facilitate the transport of electrolyte, and the thin walls shorten the Li diffusion distances. Such photonic structures were later utilized for a real electrochemical cell system, in which the anode is 3DOM carbon and the pores are filled with polymer electrolyte.[73] The top surface of the 3DOM carbon is removed so that only electrolyte is in contact with the V_2O_5 gel cathode and the bottom carbon is adhered to the current collector. This work clearly demonstrates the feasibility of constructing three-dimensional electrochemical cells based on nanostructured materials. Other highly porous materials include mesoporous vanadium oxide with nanometer-sized pores that permit the easy diffusion of lithium ions. Liu et al. synthesized mesoporous vanadium oxide with pore sizes ranging from 3 to 4 nm by electrodepositing from a $VOSO_4$ solution in the presence of a block polyalkylene oxide polymer (P123).[74] This polymer surfactant plays a key role in the formation of mesoporous structure. The authors specifically investigated the rate performance of the mesoporous vanadium oxide electrode and found that the material delivered a capacity of $125\,mA\,h\,g^{-1}$ at a high rate of 50°C, corresponding to a capacitance of $450\,F\,g^{-1}$, which is comparable to that of porous carbon capacitors. Therefore, the mesoporous vanadium oxide is very promising as cathode material for high-power lithium-ion batteries and fills the gap between batteries and capacitors. Moreover, the mesoporous structure provides elasticity that allows for dimensional change during Li-ion intercalation–deintercalation, and thus offers good cycleability.

Hydrothermal synthesis is another powerful tool to transform transition metal oxides into high-quality nanostructures, and nanostructured vanadium oxides in different morphologies can be produced via this procedure. Examples include long beltlike nanowires growing along the [010] direction,[75] and new types of belts exhibiting a boomerang shape.[76] The structure of these nanobelts is unique in that it originates from twinning along the [130] direction, which is the first observation of twins within individual nanosized crystals. Vanadium pentoxide nanobelts have been prepared to be used as highly selective and stable ethanol sensor materials by acidifying ammonium metavanadate followed by hydrothermal treatment.[77] In a separate report, $V_2O_5 \cdot n H_2O$ crystalline sheets, the intermediate products between nanobelts and nanowires, were fabricated hydrothermally using V_2O_5, H_2O_2, and HCl.[78] Nevertheless, the intercalation properties of these vanadium oxide nanobelts or nanosheets were not investigated further. More recently, Li et al. have studied the synthesis and electrochemical behavior of orthorhombic single-crystalline V_2O_5 nanobelts.[79] The V_2O_5 nanobelts with widths of 100–300 nm, thicknesses of 30–40 nm, and lengths up to tens of micrometers are obtained by hydrothermal treatment of aqueous solutions of V_2O_5 and H_2O_2. The authors proposed a dehydration–recrystallization–cleavage mechanism for the formation of V_2O_5 nanobelts. A high initial discharge capacity

of 288 mA h g^{-1} is found for the V_2O_5 nanobelts in a voltage range of 4.0–1.5 V; subsequently, the capacity decreases to 191 mA h g^{-1} for the second cycle, and then remains steady for the next four cycles. Apart from anhydrous crystalline V_2O_5 nanobelts, $V_2O_5 \cdot 0.9H_2O$ nanobelts, and $V_2O_5 \cdot 0.6H_2O$ nanorolls are synthesized with hydrothermal treatment of NH_4VO_3 in the presence of difference acids.[80] The $V_2O_5 \cdot 0.9H_2O$ nanobelts are tens of micrometers long, 100–150nm wide, and 20–30 thick. The $V_2O_5 \cdot 0.6H_2O$ nanorolls are half-tube nanostructured as a result of incomplete scrolling. It is interesting to note that $V_2O_5 \cdot 0.6H_2O$ nanorolls show higher intercalation capacity (253.6 mA h g^{-1}) than $V_2O_5 \cdot 0.9H_2O$ nanobelts (223.9 mA h g^{-1}) under a current density of 0.6 mA g^{-1}, which can be ascribed to the higher surface area and lower water content of nanorolls. Furthermore, the capacities of nanorolls and nanobelts increases to 287.8 mA h g^{-1} and 307.5 mA h g^{-1}, respectively, after annealing and dehydration of these nanostructures, which suggests a significant effect of the water content on the electrochemical behavior. Single-crystalline nanowires can also be achieved by a combination of hydrothermal process of polycrystalline V_2O_5 and post-calcination treatment.[81] The nanowires have a diameter of 50–200 nm and a length up to 100 μm, and deliver high initial capacity of 351 mA h g^{-1}. A combination of a hydrothermal method and a post-annealing process was also used by Lutta et al. to obtain vanadium oxide nanofibers.[82] In their method, polylactide fibers were hydrothermally treated in a mixture of ammonium vanadate and acetic acid followed by annealing in oxygen, resulting in vanadium oxide nanofibers 60–140 nm in width and several micrometers in length. The V_2O_5 nanofibers deliver capacities exceeding 100 mA h g^{-1} that remain stable over 10 cycles. Obviously, morphology and water content have a significant effect on the electrochemical performance of nanostructured vanadium oxides. For certain morphologies, size is another factor affecting the electrochemical properties. In this regard, Cui and co-workers prepared V_2O_5 nanoribbons and investigated the dependence of the electrochemical properties on the width and thickness of nanoribbons by studying the chemical, structural, and electrical transformations of V_2O_5 nanoribbons at the nanometer level.[83] They found that transformation of V_2O_5 into the ω-$Li_3V_2O_5$ phase takes place within 10 s in thin nanoribbons, and that efficient electronic transport can be maintained to charge ω-$Li_3V_2O_5$ nanoribbon within less than 5 s. Therefore, it is suggested that the Li diffusion constant in nanoribbons is faster than that in bulk materials by three orders of magnitude, leading to a remarkable enhancement in power density (360 °C). It can be concluded that lithium-ion batteries based on nanostructured vanadium oxides not only have higher energy densities but also higher power densities, and thus will find application in electric and hybrid electric vehicles.

3.2. Nanostructured Manganese Oxides

Apart from traditional nanostructured layered materials that intercalate guest species between the interlayers, there are other inorganic compounds demonstrating high lithium storage capacity by electrochemically reacting with lithium ions. For example, the lithium intercalation of nanostructured manganese oxide involves formation/decomposition of lithium oxide, which is facilitated by formation of metallic manganese. Interestingly, nanostructured manganese oxides can act as either cathode or anode material by controlling the working voltage range. Arrays of amorphous MnO_2 nanowires have been prepared by anodic electrodeposition into alumina templates.[84] These MnO_2 nanowires function as rechargeable cathodes for lithium-ion battery cells and deliver a capacity of 300 mA h g^{-1} when cycled between 3.5 and 2 V versus Li/Li^+. More recently, Wu's group have reported the electrochemical synthesis of interconnected MnO_2 nanowires without using any template or catalyst.[85] These interconnected MnO_2 nanowires act as cathode materials when cycled to a middle voltage (1.5 V versus Li/Li^+). When further cycled to a low voltage (0 V versus Li/Li^+), such nanostructures exhibit a high capacity of over 1000 mA h g^{-1}, higher than that of commercially used carbon families as anode materials.

In addition to MnO_2 nanowires, nanostructured MnO_2 of different crystallographic types and morphologies has been synthesized through solution routes and investigated as Li-ion battery cathode materials. Nanocrystals of α-, β-, and γ-MnO_2 could be synthesized by using simple hydrothermal decomposition of a $Mn(NO_3)_2$ solution.[86] Typically, β-MnO_2 crystals are produced with a variety of novel shapes, including one-dimensional nanowires, two-dimensional hexagonal star-like structures, and dendritic hierarchical nanostructures. However, β-MnO_2 nanostructures show low capacity and poor cycling stability, while α- and γ-MnO_2 one-dimensional nanostructures demonstrate favorable electrochemical performance. α-MnO_2 nanowires deliver a capacity of 204 mA h g^{-1} when discharged to 1.5 V versus Li/L^+ and retain a capacity of 112 mA h g^{-1} after 20 cycles at a current rate of 50 mA g^{-1}. γ-MnO_2 nanorods deliver a capacity of more than 210 mA h g^{-1} and retain a capacity of 148 mA h g^{-1} after 20 cycles at the current rate of 50 mA g^{-1}. In another report, Ho and Yen prepared α-/γ-MnO_2 mixed-phase coating on Pt through cathodic deposition from $Mn(NO_3)_2$ aqueous solution.[87] The morphology of such α-/γ-MnO_2 coating resembles a honeycomb consisting of flake structures on the nanometer scale. Remarkably, the α-/γ-MnO_2 coating shows a gradual increase in capacity and crystalline stability after cyclic test. Its Li-intercalation capacity increases from 182 mA h g^{-1} for the first cycle to 209 mA h g^{-1} for the tenth cycle between 4.0 and 2.0 V versus Li/Li^+. Such enhancement in capacity and crystallization after cycling is ascribed to the mixed α-/γ-MnO_2 phases and the nanometer-sized structure. As mentioned above, bulk β-MnO_2 or nanostructured β-MnO_2 rapidly converts to $LiMn_2O_4$ spinel upon Li intercalation, resulting in unfavorable electrochemical performance. However, mesoporous β-MnO_2 demonstrates a remarkably high Li intercalation capacity of 284 mA h g^{-1}, corresponding to a composition of $Li_{0.92}MnO_2$.[88] Bruce's group reported the first synthesis of mesoporous β-MnO_2 with a highly ordered pore

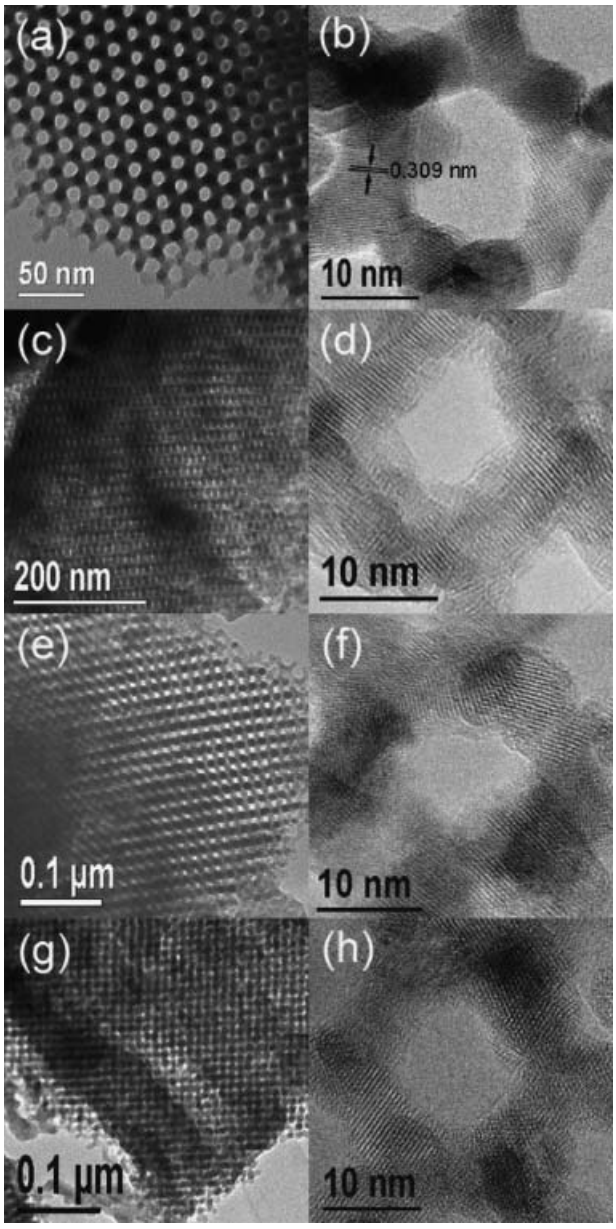

Figure 6. TEM and high-resolution TEM images of mesoporous β-MnO_2: a,b) as-prepared; c,d) after discharge; e,f) end of discharge after 30 cycles; and g,h) end of charge after 30 cycles.

structure and highly crystalline walls.[88] Figure 6a and b shows typical TEM images of mesoporous β-MnO_2, clearly demonstrating the highly ordered pore structure with a wall thickness of 7.5 nm. Figure 6c–h shows TEM images of mesoporous β-MnO_2 after first charge, end of discharge after 30 cycles, and end of charge after 30 cycles. Both the β-MnO_2 crystal structure and the mesoporous structure are preserved upon cycling. The thin walls of the mesoporous β-MnO_2 allow volume changes during Li intercalation–deintercalation, and 81% capacity is retained after 50 cycles. High capacities of more than 230 mA h g^{-1} are also reported for layered MnO_2 nanobelts, synthesized by Ma et al. using the hydrothermal treatment of Mn_2O_3 powders in an aqueous solution of NaOH.[89] The nanobelts self-assemble into bundles with narrow size dispersion of 5–15 nm width and demonstrate a high capacity of 230 mA h g^{-1} up to 30 cycles.

Amorphous manganese oxides have also received increasing attention as cathode materials used in lithium-ion batteries.[90,91] Yang and Xu prepared nanostructured amorphous MnO_2 cryogels using two different sol–gel routes and investigated the influence of synthesis conditions on their electrochemical properties.[92] The cryogels are obtained by freeze-drying MnO_2 hydrogels and the hydrogels are synthesized by reacting sodium permanganate with disodium fumarate (route 1) or with fumaric acid (route 2), respectively. Cryogels obtained from hydrogels synthesized via route 2 deliver much higher Li intercalation capacities than those obtained from hydrogels synthesized via route 1. For both routes, cryogels obtained from hydrogels using higher precursor concentration exhibit higher capacities. The capacity of the cryogel with the best performance can reach 289 mA h g^{-1} at a C/100 rate.

4. Nanosized Coatings on Cathode Materials

4.1. Nanosized Coatings on Lithium Transition Metal Oxides

It should be noted that the nanoparticulate forms of lithium transition metal oxides such as $LiCoO_2$, $LiNiO_2$, or their solid solutions can react with the electrolyte and lead to safety problems. In the case of $LiMn_2O_4$, the use of nanoparticles causes undesirable dissolution of Mn. Significant efforts have been made to increase the stability of these nanocrystalline lithium metal oxides. Better stability can be achieved by coating the electrode materials with a nanosized stabilizing surface layer that alleviates these problems.

As for $LiCoO_2$, coatings of various phosphates and oxides have been studied and significant improvements in capacity retention have been demonstrated. Kim et al. made an extensive study on the effect of the MPO_4 (M = Al, Fe, SrH, and Ce) nanoparticle coatings on $LiCoO_2$ cathode materials.[93] They found that the extent of the coating coverage is affected by the nanoparticle size and morphology despite the same coating concentration and annealing temperature. Smaller nanoparticles of $AlPO_4$ or $FePO_4$ with a size less than 20 nm fully encapsulate $LiCoO_2$, whereas $CePO_4$ particles with a size larger than 150 nm or whisker-shaped $SrHPO_4$ only partially cover $LiCoO_2$. Not surprisingly, the $LiCoO_2$ fully covered by $AlPO_4$ or $FePO_4$ exhibits the highest intercalation capacity of 230 mA h g^{-1} in a voltage range of 4.8 and 3 V at a rate of 0.1°C. The $AlPO_4$-coated $LiCoO_2$ also shows the best capacity retention. Nevertheless, the $CePO_4$- and $SrHPO_4$-coated cathodes shows better capacity retention than the $FePO_4$-coated cathode at 90 °C, which is attributed to the continuous Fe metal ion dissolution at this temperature.

The improvement in the electrochemical performance in the coated cathode is ascribed to the suppression of cobalt dissolution and the non-uniform distribution of local strain by the coating layer. In a further investigation of $AlPO_4$-coated $LiCoO_2$, electrochemical properties of $AlPO_4$-nanoparticle-coated $LiCoO_2$ at various cut-off voltages were found to depend on the annealing temperature.[94] The $AlPO_4$-coated cathodes exhibit excellent electrochemical performance with high cut-off voltages, larger than 4.6 V, when annealed at 600 and 700 °C, while such cathodes annealed at 400 °C show a lower capacity and poorer rate capability. However, the $AlPO_4$-coated $LiCoO_2$ annealed at 400 °C showed optimal capacity retention.[95] Figure 7 shows typical TEM images of $AlPO_4$-coated $LiCoO_2$ deposited at room temperature, 400 °C and 700 °C. A continuous layer of $AlPO_4$ with thickness of about 100 nm is coated on the surface of $LiCoO_2$, as shown in Figure 7a. The coating layer deposited at room temperature is amorphous (Fig. 7b). The coating deposited at 400 °C is composed of nanocrystals with size in the range of 3–5 nm (Fig. 7c), and the coating deposited at 700 °C consists of nanocrystals ca. 20–30 nm in size (Fig. 7d). The dependence of electrochemical properties on annealing temperature can be explained by the effect of temperature on the nanostructures of the coating layer and the interdiffusion at the interface between the coating layer and the $LiCoO_2$ cathode. In addition to coatings of phosphates, surface modification of $LiCoO_2$ by coating various oxides such as ZrO_2,[96] Al_2O_3,[97] SnO_2,[98] MgO,[99] or ZnO[100] has been widely investigated. In the case of ZnO-coated $LiCoO_2$, the ZnO coating reduces the cobalt dissolution and prevents the inorganic surface films such as LiF from covering the $LiCoO_2$ particles.[101] Moreover, the ZnO coating alleviates the cycle-life degradation caused by inappropriate conductive carbon. Based on the impedance spectra, the charge-transfer resistance of ZnO-coated $LiCoO_2$ is much smaller than of the uncoated cathode, although the ZnO coating layer is more resistant than the $LiCoO_2$ surfaces. It can be concluded that surface modification with ZnO improves the high-voltage cycleability of the $LiCoO_2$ cathodes. In a similar manner, ZrO_2 coating protects the $LiCoO_2$ cathode surface and reduces the electrolyte decomposition at high voltages.[102,103] The ZrO_2-coated $LiCoO_2$ shows much better structural change behaviors than the bare $LiCoO_2$, as evidenced by in situ XRD data. The battery cells discussed above all employ liquid organic electrolytes that are flammable and cause safety concerns. Replacing the liquid electrolyte with nonflammable solid electrolyte such as sulfide electrolyte is a solution to these safety problems, however, the energy densities and power densities of solid-state lithium batteries are relatively low for practical applications. One way to improve the rate capability of solid-state batteries is to add a buffer film, with a thickness on the nanometer scale, between the electrode and electrolyte materials. A thin layer of $Li_4Ti_5O_{12}$ with thickness of a few nanometers was chosen to be coated on the $LiCoO_2$ cathode.[104] The $Li_4Ti_5O_{12}$ is also a Li intercalation material that ensures the electronic conduction, however, this material intercalates lithium ions at voltages lower than 1.5 V and thus does not act as intercalation material in the voltage range of $LiCoO_2$. The power densities of the solid-state batteries with the thin $Li_4Ti_5O_{12}$ layer between the $LiCoO_2$ cathode and sulfide electrolyte are greatly increased and comparable to those of commercial lithium batteries, which is attributed to the suppression of lithium-ion transfer.

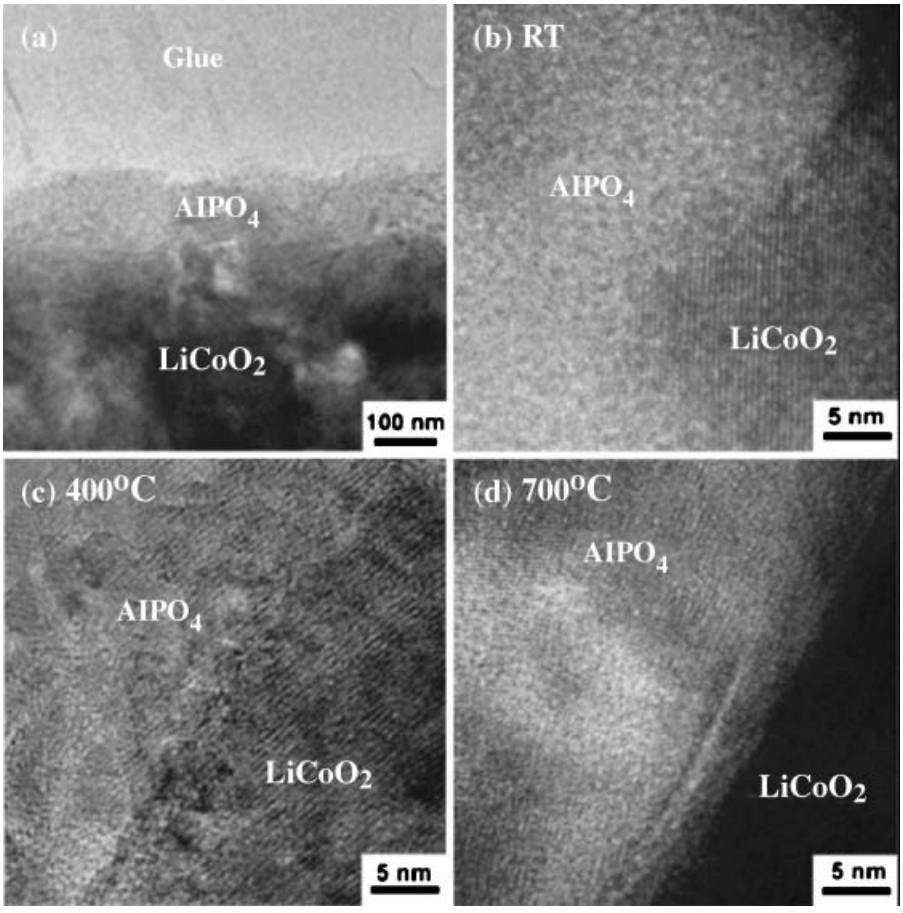

Figure 7. a) Cross-sectional TEM images of $AlPO_4$-coated $LiCoO_2$. A ca. 100 nm thick $AlPO_4$ continuous layer is coated on $LiCoO_2$. High-resolution images of the AlPO4-coated $LiCoO_2$ at b) room temperature, c) 400 °C, and d) 700 °C. Adapted with permission from [95]. Copyright 2006 The Electrochemical Society.

$LiMn_2O_4$ or substituted $LiMn_2O_4$ is very attractive as a cathode material

because it is safer and cheaper than $LiCoO_2$. However, this material suffers from capacity fading, especially at elevated temperatures. Coating of nanosized oxides on $LiMn_2O_4$ will help to improve its cycling performance. The electrochemical behavior of nanosized ZnO-coated $LiMn_2O_4$ was examined at 55 °C.[105] After 50 cycles at 55 °C, the coated $LiMn_2O_4$ shows capacity retention of 97%, much higher than the capacity retention (58%) of the bare cathode. ZnO coating collects HF from the electrolyte and thus decreases the Mn dissolution in the electrolyte, then subsequently reduces the interfacial resistance. For the same reason, nanometer-sized ZnO homogenously coated on the $Li_{1.05}Al_{0.1}Mn_{1.85}O_{3.95}F_{0.05}$ by a hydrothermal process was found to significantly improve cycling performance of the cathode at 55 °C.[106] The coated $Li_{1.05}Al_{0.1}Mn_{1.85}O_{3.95}F_{0.05}$ shows high capacity retention of 98.5% after 50 cycles. Similarly, coating of amorphous ZrO_2 on $LiMn_2O_4$ can improve the high-temperature cycleability by picking up acidic species from electrolyte.[107] Moreover, the ZrO_2-coated $LiMn_2O_4$ exhibits tremendously improved cycling stability at high rates up to 10 °C owing to the following mechanisms. First, ZrO_2 can form several stable phases with Li and, thus, amorphous ZrO_2 matrix possibly possesses a high solubility of Li. Therefore, the ZrO_2 coating can act as a highly Li-conducting solid electrolyte interface, which reduces the interfacial resistance. Second, the rigid oxide coating strongly bonds to $LiMn_2O_4$, which tolerates the lattice stress resulting from volume expansion during lithium intercalation. Lastly, ZrO_2 can collect HF from electrolyte to reduce Mn dissolution like ZnO does. The electrochemical behavior of ZrO_2-coated stoichiometric $LiMn_2O_4$ and substituted $Li_{1.05}M_{0.05}Mn_{1.9}O_4$ (M = Al, Ni) cathodes were further compared with those of cathodes coated with Al_2O_3 and SiO_2. ZrO_2-coated $Li_{1.05}M_{0.05}Mn_{1.9}O_4$ (M = Al, Ni) shows the best cycling stability at 50 °C.[108] The ZrO_2 coating, deposited from colloidal suspensions, is a porous network connected by ZrO_2 nanoparticles with dimensions less than 4 nm. This ZrO_2 network effectively scavenges HF from the electrolyte and allows the access of the electrolyte to the cathode, and thus improves the high-temperature cycleability of the cathode.

4.2. Nanosized Coatings on Lithium Phosphates

Lithium phosphate is presently at the center of much interest as cathode for lithium-ion batteries, because it is inexpensive, abundantly available, environmentally friendly, thermally stable in the fully charged state, and has a large theoretical capacity of 170 mA h g^{-1}. The results on the diffusion coefficient of $LiFePO_4$ are controversial, because there is no compositional variation and what is measured is the movement of the $LiFePO_4/FePO_4$ interface. A diffusion coefficient around 10^{-13}–10^{-14} cm^2 s^{-1} over a whole range of composition was reported by Franger et al. for $LiFePO_4$.[109] Another experimental work reported a value of 2×10^{-14} cm^2 s^{-1}.[110] Most recently, a systematic study of $LiFePO_4$ with cyclic voltammetry (CV) has been presented.[111] In this study, the lithium diffusion coefficients were determined by CV to be 2.2×10^{-14} and 1.4×10^{-14} cm^2 s^{-1} for charging and discharging $LiFePO_4$ electrodes in 1 M $LiPF_6$ ethylene carbonate/diethyl carbonate, respectively. There are essentially no electronically conducting species in pure $LiFePO_4$. Therefore, the conductivity of the material is only 10^{-11} S cm^{-1}, partially owing to the motion of lithium ions.[112] Carbon-containing precursors (e.g., carbonates, acetates, and oxalates) are used to prepare $LiFePO_4$ so that some residual carbon will prevent the formation of ferric ions. The as-prepared samples show higher conductivities, in the range of 10^{-5}–10^{-6} S cm^{-1}, however, it is not yet high enough for high power lithium batteries.[113]

To increase the conductivity, the material could be doped as suggested by Chiang and co-workers.[112] However, doping may have deleterious impact if it occurs on the lithium sites. Conductive coatings deposited on the surface of $LiFePO_4$ are usually employed to solve the conductivity issue. Most coatings are carbonaceous and deposited during the synthesis process. Pioneering work on carbon-coated $LiFePO_4$ was carried out by Ravet et al.[114,115] Sucrose was used as one carbon source[115] and was added on the initial hydrothermal samples[116] or during pyrolysis.[117] Other methods include thermal decomposition of pyrene[118] or citric-acid-based sol–gel processing.[119] It should be noted that the electrochemical properties of $LiFePO_4$ are influenced by the quality of carbon coatings. Wilcox et al. found that the conductivity and rate behavior of $LiFePO_4$ are strongly affected by carbon structural factors such as sp^2/sp^3 and disordered/graphene (D/G), as determined by Raman spectroscopy and H/C ratios determined from elemental analysis.[120] The structure of carbon can be controlled by the use of additives during $LiFePO_4$ synthesis. $LiFePO_4$ coated with the more graphitic carbon has higher conductivity and shows better electrochemical performance. Another factor that influences the electrochemical performance of $LiFePO_4$/C composites is the porosity. Gaberscek et al. prepared microsized porous $LiFePO_4$/C particles with different morphologies by using different techniques such as solid-state or sol–gel methods.[121] The composite porosity is influenced by synthesis and synthesis parameters. The composites prepared at a relatively high heating rate (>5 K min^{-1}) have interconnected pores and show the best electrochemical performance, e.g., more than 140 mA h g^{-1} at C/2 rate during continuous cycling.

In addition to carbon coating, metal coating such as silver has been successfully used to increase the conductivity as well.[122] Another type of coating is conductive inorganic layer such as metallic Fe_2P, as investigated by Rho et al.[123] In their study, mixture of Fe_2P and FeP were deposited on the surface of the $LiFePO_4$ along with carbon and the byproduct Li_3PO_4 by surface reduction reactions. Fe_2P is coated directly on the $LiFePO_4$, while carbon and Li_3PO_4 sit on the outer surface of the crystallites. Such surface layer structure facilitates significantly improved rate capabilities and superior cycleability: a high capacity of 105 mAh g^{-1} is achieved at a very high rate of 14.8 °C. Recently Wang and Su's group have designed a $LiFePO_4$ spherical structure coated by a π-bond character planar polymer – polyacene (PAS) – by pyrolysis of

the phenol-formaldehyde resin.[124] The conductivity of the $LiFePO_4$-PAS structure is drastically increased to $10\,S\,cm^{-1}$. High capacities and excellent cycling performance are achieved for the $LiFePO_4$-PAS structure in a wide temperature range of –20 to 60 °C. In another study presented by Goodenough's group, the conductive polymer polypyrrole (PPy) was bonded to $LiFePO_4$ particles by a carbon coat and was found to significantly improve the capacity and rate capability of $LiFePO_4$.[125] For example, at a high rate of 10 C, the C-$LiFePO_4$/PPy containing 16 wt % PPy shows a high capacity and steady cycling performance. In a similar manner, electronically conducting RuO_2 was used as an oxidic nanoscale interconnect for carbon containing porous $LiFePO_4$ to improve electrode performance.[126] RuO_2 with a particle size of about 5 nm was deposited on the carbon-$LiFePO_4$ with an average pore size of 50 nm by using cryogenic decomposition of RuO_4 at low temperature. The resulting C-$LiFePO_4$/RuO_2 composite maintains the morphology and structure of the original C-$LiFePO_4$, as revealed by high-resolution TEM images in Figure 8. Nanosized RuO_2 as an oxide adheres well with oxides such as $LiFePO_4$, while simultaneously assuring good contact with carbon. Hence, RuO_2 repairs incomplete carbon network in porous $LiFePO_4$ and thus improves the kinetics and rate capability of the composite. It is found that the original C-$LiFePO_4$ electrode shows decent performance at low current rates but the performance deteriorates at high current rates. The C-$LiFePO_4$/RuO_2 shows improved electrochemical behavior at high rates.

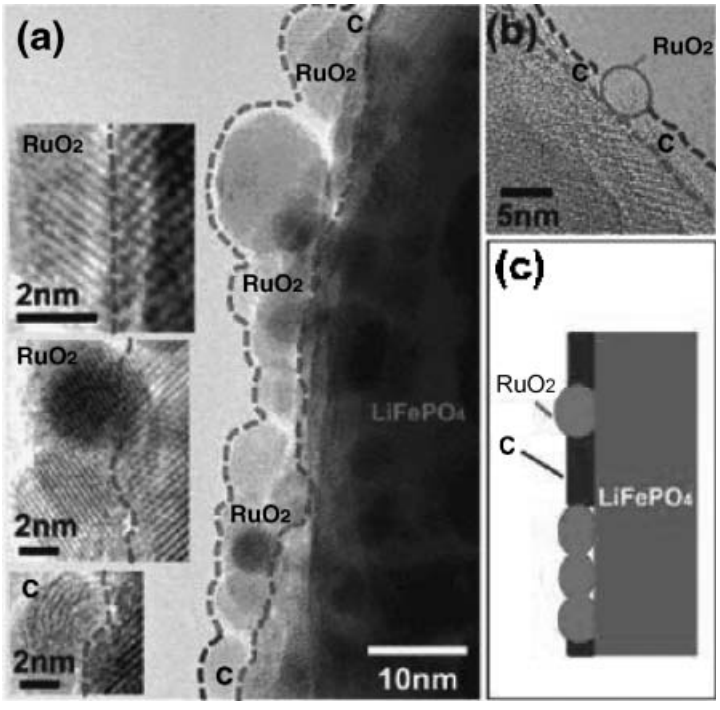

Figure 8. a,b) High-resolution TEM images of C-$LiFePO_4$ after RuO_2 coating. c) Schematic of the repair of the electronically conducting network of carbon on porous $LiFePO_4$ by nanosized RuO_2.

The problems of low electronic conductivity and slow diffusion of lithium ions in $LiFePO_4$ can be further alleviated by modifying with conductive species and by minimizing particle size simultaneously, for example, a nanocomposite of $LiFePO_4$ with a carbon xerogel could be formed from a resorcinol-formaldehyde precursor. This nanocomposite achieves 90% theoretical capacity at C/2 with very good stability at room temperature.[127] Such excellent electrochemical performance is attributed to modification with carbon and control of particle size to nanometer scale. Both factors are of essential importance. The nanosized $LiFePO_4$/carbon composites with dimensions in the range of 20–30 nm could also be prepared by using citric acid as a complexing agent and a carbon source, which suppresses the growth of $LiFePO_4$ particles and enhances the conductivity of the composites a sol–gel method.[128] The carbon-coated $LiFePO_4$ sintered at 850 °C demonstrates the highest conductivity of $2.46 \times 10^{-3}\,S\,cm^{-1}$ and best electrochemical properties, as shown in Figure 9. The discharge profile is flat over a wide voltage range, due to the two-phase redox reaction via a first-order transition between $FePO_4$ and $LiFePO_4$.[129] A discharge capacity of 148 mA h g^{-1} is achieved for this cathode material. A slight increase in capacity is observed after a few cycles, showing good cycleablity.

5. Nanostructured Composites

As noted above, most cathode materials with interesting thermodynamic properties are typically ceramic materials with low electronic conductivity ranging from $10^{-3}\,S\,cm^{-1}$ for $LiCoO_2$[40] down to $10^{-9}\,S\,cm^{-1}$ for $LiFePO_4$.[112] To improve the electrochemical kinetics, the cathode materials need to be embedded within an electronically conducting network, for example, some thin coating of conductive material. The coatings must be thin enough, on the nanoscale, so that ions can penetrate through them without appreciable polarization. Furthermore, the internal electrical field generated by electrons may enhance the ionic motions.[130] Such surface modifications alleviate the problem of low electronic conductivity, at the same time, reducing the size of active material would shorten the diffusion length for lithium. The realization of such nanostructured composites consisting of cathode materials and conductive additives makes it possible to utilize theoretical capacities at intermediate or even higher rates.

5.1. Nanostructured Carbon-Oxide Composites

One of the commonly studied carbon-based composites is the carbon/vanadium oxide composite. Carbon-coated V_2O_5 nanoparticles can be synthesized via burning off carbon-coated V_2O_3 nanoparticles around 400 °C in air.[131] The thickness and weight percentage of carbon can be manipulated by varying the conditions of the burning process. The optimal carbon content is

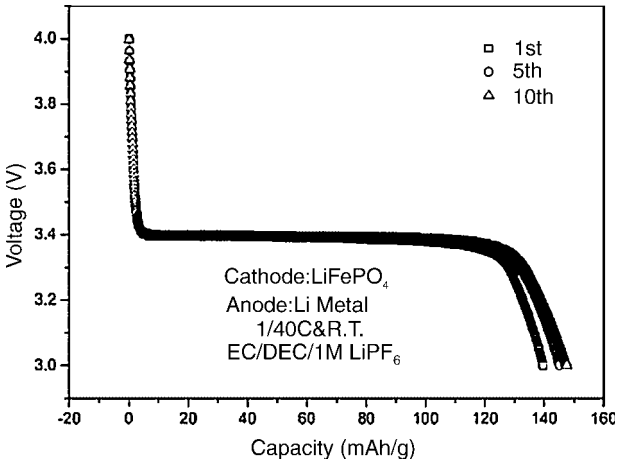

Figure 9. Discharge curves of $LiFePO_4$/carbon sintered at 850 °C for 2 hours. Adapted with permission from [128]. Copyright 2004 Royal Society of Chemistry.

found to be 2–3% by weight. Because of the carbon coating, these C-V_2O_5 nanoparticles have good interparticle electrical contact, and do not have the usual drawbacks of nanoparticles such as poor active mass integrity and high surface reactivity. Therefore, carbon-coated V_2O_5 nanoparticles are found to a have higher capacity, better rate capability, and better cycleability than V_2O_5 microparticles or nanoparticles. The Li intercalation capacity of C-V_2O_5 nanoparticles reaches 290 mA h g^{-1} at high rates.

Higher capacities can be achieved with vanadium oxide/carbon nanotube nanocomposites. Dunn's group incorporated V_2O_5 aerogels into single-walled carbon nanotubes using a sol–gel method.[132] The carbon nanotubes and V_2O_5 nanoribbons in the aerogel have similar morphology and dimensional scale, and thus have intimate contact with each other on the nanoscale. Moreover, the porous structure of carbon nanotubes and V_2O_5 aerogel permits electrolyte access throughout the composite material. As a result, such nanocomposite electrode shows high capacities exceeding 400 mA h g^{-1} at high rates.

Apart from vanadium oxides, some nanostructured lithium vanadium oxides have also been reported to form nanocomposite with carbon, which exhibits excellent electrochemical characteristics. It was reported that mixing the precursor of $Li_{1+\alpha}V_3O_8$ with a suspension of carbon black resulted in nanocomposites of $Li_{1+\alpha+x}V_3O_8/\beta$-$Li_{1/3}V_2O_5$/C.[133] β-$Li_{1/3}V_2O_5$ was a byproduct formed when the initial $Li_{1+\alpha}V_3O_8$ was reduced by carbon. Here carbon particles play critical roles as a reducing agent, a growth-limiting agent to restrict the electroactive material within the nanoscale, and as an electronically conducting agent. The $Li_{1+\alpha+x}V_3O_8/\beta$-$Li_{1/3}V_2O_5$/C nanocomposite shows significantly better electrochemical performance in comparison with the standard $Li_{1+\alpha}V_3O_8$. Similarly, acetylene black was used to prompt the reduction of potassium permanganate, yielding amorphous manganese oxide/carbon composites.[134] The as-prepared composite delivers a high capacity of 231 mA h g^{-1} at a current density of 40 mA g^{-1}, showing good electrochemical performance at high rates.

The energy density of MnO_2/C nanocomposite can be further increased by optimization of the synthesis conditions. The MnO_2/C nanocomposite can be obtained via a sonochemical synthesis method using acetylene black and sodium permanganate. Synthesis conditions such as the reaction temperature and specific surface area of the carbon have been optimized to achieve the best electrochemical performance of the nanocomposite.[135] The active material content increases by increasing the reaction temperature. It is interesting to note that the capacity increases with the increasing amount of active material then decreases, because the excessive formation of active material increases the electrochemicaly effective volume, leading to capacity drop. On the other hand, using carbon with higher surface area results in higher capacity; the highest capacities are 126 and 99.9 mA h g^{-1} at current densities of 1 and 10 A g^{-1}, respectively. A number of lithium phosphates/carbon composites have also been studied as cathode materials for lithium batteries, including those of general formula $LiMPO_4$ (M = Fe, Mn, Co, Ni)[136] and $Li_3V_2(PO_4)_3$.[137] Among the carbon-coated $LiMPO_4$ (M = Fe, Mn, Co, Ni) composites, the $LiFePO_4$/C with surface carbon coating of 1.8 wt % achieves an electronic conductivity of 10^{-2} S cm^{-1} and shows the best electrochemical performance.

Compared to $LiFePO_4$, which attracts a lot of attention, $Li_3V_2(PO_4)_3$ is relatively unexplored. Similar to $LiFePO_4$, this material also suffers from low electronic conductivity. To solve this issue, $Li_3V_2(PO_4)_3$ crystallites were wrapped within a conductive carbon network to form a nanocomposite that delivers almost full capacity at high rates.[137] The potential curves in Figure 10a reveal that two lithium ions per formula unit are completely extracted in three steps to give a theoretical capacity (100%) of 132 mA h g^{-1} at a rate of C/5. 95% theoretical capacity is still achieved at a high rate of 5 C. The flat plateaus in the curve correspond to $Li_xV_2(PO_4)_3$, where $x = 2.5$ (i); 2.0 (ii); and 1.0 (iii), as shown in Figure 10a. Such a sequence of phase transitions between two single phases shows the very low degree of polarization in the discharge curve owning to the facile ion and electron transport. Excellent cycling stability is also demonstrated by this material, as shown in Figure 10b. When cycled between 3.0 V and 4.8 V, the $Li_3V_2(PO_4)_3$/C composite delivers a specific energy density of 2330 mW h cm^{-3}, comparable to $LiCoO_2$ (2750 mW h cm^{-3}) or $LiFePO_4$ (2065 mW h cm^{-3}).

5.2. Nanostructured Polymer-Oxide Composites

Over the past two decades much interest has been placed on conductive polymer/transition metal oxide nanocomposites. These hybrid material consist of conductive organic polymers (e.g., polyacetylene, polyaniline, and PPy) interleaved between the layers of an oxide lattice such as V_2O_5. Both oxide and

ADVANCED MATERIALS

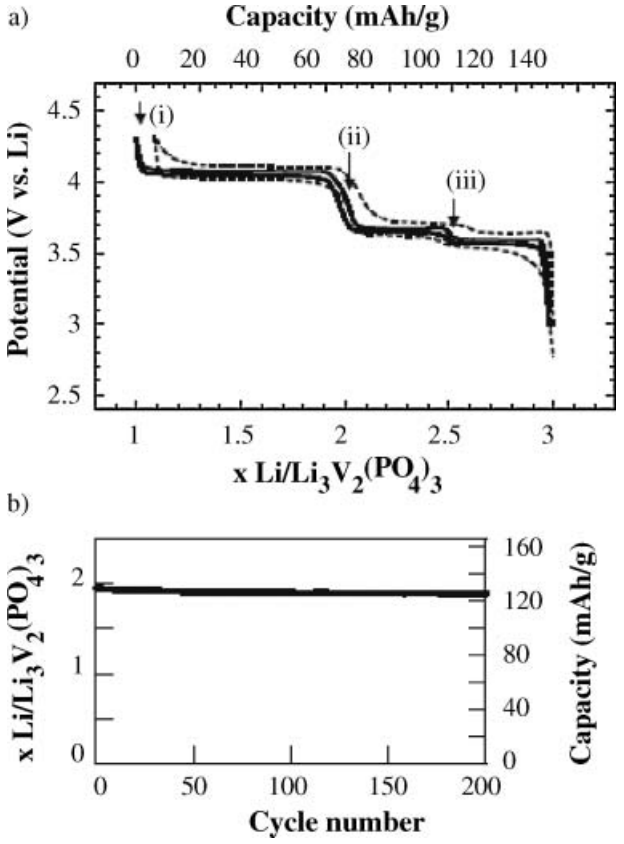

Figure 10. a) Voltage-composition plot for C-$Li_3V_2(PO_4)_3$ composites at rates of C/5 (solid line) and 5C (dotted line) in the potential window 3.0–4.3 V; single phase compositions are indicated: $x = 2.5$ (i); 2.0 (ii); and 1.0 (iii). b) Cycling stability at a rate of 1°C.

polymer are electrochemically active, and this feature makes the polymer/oxide nanocomposite very attractive as the cathode material for lithium batteries. The layer-by-layer (LbL) technique, based on physical adsorption of oppositely charged layers, has been widely used to prepare V_2O_5 nanocomposites alternating with polymer layers. One popular example is the V_2O_5/polyaniline nanocomposite film fabricated by the LbL technique, and the intimate contact between the oxide and polymer on the nanoscale results in an improved intercalation capacity.[138] Later, a V_2O_5 nanocomposite alternating with blends of chitosan and poly(ethylene oxide) (PEO) was prepared using the LbL technique and investigated the charge storage capability in such nanoarchitectures.[139] A small amount of chitosan (1%) is added to blend with PEO because the adsorption of alternate layers of PEO and V_2O_5 is not efficient. The V_2O_5/blend shows higher capacity and intercalates 1.77 moles of lithium per mole of V_2O_5. The enhanced electrochemical performance of V_2O_5/blend in comparison with V_2O_5/chitosan is due to a larger number of electrochemically active sites and faster lithium diffusion within the host material. At 20 mV s^{-1}, the charges injected were 3.29 mC cm^{-2} and 8.02 mC cm^{-2} for the V_2O_5/chitosan and V_2O_5/blend, respectively. In a more recent report, polyaniline homogeneously distributed into a V_2O_5/polyaniline nanocomposite was found to stabilize the capacity.[140] In this study, a reverse micelle method was used to prepare V_2O_5/polyaniline nanofibers that exhibit improved cycling performance compared to the V_2O_5 nanofibers.[140] The V_2O_5/polyaniline nanofibers containing 30 mol % polyaniline deliver a steady capacity of about 300 mA h g^{-1} without morphology change over 10 cycles, whereas the V_2O_5 nanofibers do not retain the morphology after cycling. Some V_2O_5/polymer nanocomposites show lower storage capacity but better cycling stability compared to pure nanostructured V_2O_5.[141] As reported by Reddy et al., $PVP_xV_2O_5$ ($x = 0.5$, 1) nanobelts synthesized by a hydrothermal method exhibit lower capacity but better cycleability compared with V_2O_5 nanobelts. The authors studied the interaction between the oxide and polymer with Fourier transformation infrared spectroscopy (FTIR) and found that the hydrogen atoms in PVP are hydrogen-bonded with the oxygen atoms of the V = O bonds of V_2O_5 nanobelts, which effectively shields the electrostatic interaction between V_2O_5 interlayer and lithium ions. As discussed above, polymers can be intercalated between the interlayers of V_2O_5, on the other hand, V_2O_5 can be interleaved within a block polymer matrix as well.[142] Mayes and co-workers used a sol–gel method to prepare continuous and amorphous V_2O_5 phase within the poly(oligooxythylene methacrylate) (POEM) domains of a poly(oligooxythylene methacrylate)-*block*-poly (butyl methacrylate) (POEM-*b*-PBMA) copolymer (70 wt % POEM) up to weight ratios of 34% V_2O_5.[142] The resulting nanocomposite film is flexible and semitransparent and the redox activity of V_2O_5 is preserved in such nanocomposite.

Cathode materials other than V_2O_5 can form nanocomposites with conductive polymers as well. Poly(ethylene oxide) (PEO) was used as an electroactive polymeric binder to mix with carbon-containing $Li_{1.1}V_3O_8$.[143] The resulted composite electrode shows a capacity of 270 mA h g^{-1} at a rate of 5/C, higher than the capacity (180 mA h g^{-1} at C/5 rate) of the standard electrode without PEO. Such improved electrode performance is attributed to the more efficient charge-carrier collection within the composite electrode. Among all known cathode materials, elemental sulfur is the cheapest and has the highest theoretical capacity density of 1672 mA h g^{-1}, assuming a complete reaction to yield Li_2S.[144] However, Li/S cells suffer from low utilization of active material, because electrochemical reaction with the interior active materials is hindered by the insulated reaction products covering the sulfur particles. Moreover, the dissolved polysulfides transfer onto the surface of the Li anode, causing lithium corrosion and poor rechargeability of Li/S cells. To overcome these two problems, nanodispersed composites with sulfur embedded in a conductive polymer matrix were designed and prepared by heating a mixture of polyacrylonitrile (PAN) and sublimed sulfur.[145,146] The composite also show excellent cycling life owing to the suppressed dissolution of polysulfides into the electrolyte and thus demonstrates a great potential as cathode material for lithium batteries. Conductive polymers themselves can act as cathode material, however, they suffer

from low capacities and display sloping charge–discharge curves. For example, PPy is one of the most popular conductive polymers and has a specific energy ranging from 80 to 390 W h kg^{-1}.[147] To improve its capacity, a Fe^{III}/Fe^{II} redox couple is physically or chemically attached to the PPy polymer backbone.[148] The examination of the PPy/$LiFePO_4$ composite electrode shows that the composite has higher specific capacity and rate capability.

5.3. Nanostructured Metal-Oxide Composites and Other Composites

The third-most-popular composite electrode comprise metal-based cathode material, exemplified by the Ni–$V_2O_5 \cdot n H_2O$ core/shell structure discussed earlier in Section 3.1. Accordingly, Wang et al. synthesized Ag-$Ag_{0.08}V_2O_5 \cdot n H_2O$ composite films by dispersing silver nanowires into $V_2O_5 \cdot n H_2O$ matrix.[149] The composite film is found to deliver twice the capacity of the $V_2O_5 \cdot n H_2O$ xerogel film, owing to further amorphization of $V_2O_5 \cdot n H_2O$, the increased porosity, and the enhanced electronic conductivity. In a similar concept, $LiCoO_2$/Ag multilayer film was fabricated by magnetron sputtering and showed enhanced rate capability in comparison with $LiCoO_2$ film of the same thickness.[150] The thickness of the Ag layer is restricted within nanoscale and the rate capability of the multilayer film improves with the increased thickness of Ag layer as a result of the enhanced electronic conductivity.

More recently, oxide/metal/polymer composites have been obtained, showing very good electrochemical performance. One example is freestanding V_2O_5/Pt/PVA multilayer films with the thicknesses of the V_2O_5, Pt, and PVA at 22, 57, and 704 nm.[151] Other types of composite structures include oxide/oxide composite, such as a double-layer cathode composed of a $LiCoO_2$ main layer with a $LiFePO_4$ sublayer on top of an Al current collector, which shows better tolerance against overcharging than other electrodes including ($LiCoO_2$-$LiFePO_4$ mixture)/Al single layer and $LiFePO_4/LiCoO_2$/Al double layer.[152] The enhanced electrochemical performance is attributed to a large increase in the Ohmic resistance of the delithiated Li_xFePO_4 layer, which shuts the charging current down during overcharging without shut-down of the separator. The third type of composite structure is polymer/carbon nanocomposite, such as a polyaniline (PANI)/multiwalled carbon nanotube (CNT) composite synthesized via in situ chemical polymerization. This nanocomposite is utilized as a cathode material in a lithium metal-polymer cell assembled with ionic liquid electrolyte.[153] Such a cell demonstrates a maximum discharge capacity of 139 mA h g^{-1} with good cycleability and shows decent high rate performance (111 mA h g^{-1} at the 2.0 °C rate).

6. Concluding Remarks

This Review clearly reveals how moving from bulk to nanoscale materials can significantly change device performance for energy storage and conversion. The development of high-performance lithium-ion batteries can benefit from the distinct properties of nanomaterials, such as high surface areas, short diffusion paths, and large quantities of active sites, as well as freedom for volume change during charging–discharging cycles. Among a wide range of synthetic methods to prepare nanomaterials, soft chemistry routes that involve sol–gel reactions are simple and elegant and frequently use organic molecules as structure-directing templates.

As discussed in this Review, there are two groups of Li-ion battery cathode materials in general: the one with more compact lattices such as $LiCoO_2$, $LiNiO_2$, $LiMn_2O_4$, substituted lithium transition metal oxides, or solid solutions of lithium transition metal oxides, and the other group of cathode materials with a more open structure, including V_2O_5, MnO_2, and $LiFePO_4$. Nanoparticulate forms and 1D nanostructures of lithium transition metal oxides can be easily fabricated by solid-state approaches or solution chemistry methods. To increase the stability of these nanocrystalline lithium transition metal oxides, it is necessary to coat these materials with nanosized thick layers to suppress metal dissolution. In the case of $LiCoO_2$, coatings of various phosphates (e.g., $AlPO_4$) and oxides (e.g., ZnO or ZrO_2) have been studied, and significant improvements in capacity retention have been demonstrated. Nanosized ZnO or ZrO_2 coatings on $LiMn_2O_4$ and substituted $LiMn_2O_4$ also help to improve the cycling performance of the cathodes by collecting acidic species from the electrolyte to reduce Mn dissolution. Vanadium oxide is one of the oxides studied earliest for use as cathode material. There are many reports on synthesis and electrochemical properties of nanostructured vanadium oxides. Sol–gel processing and hydrothermal treatment are usually employed to prepare a large variety of nanostructured vanadium oxides, including nanorolls, nanobelts, nanowires, mesoporous structures, two-dimensional thin films with nanosized features and three-dimensional ordered photonic crystal structures with nanosized features. The template-based solution methods are utilized to prepare ordered arrays of nanostructures, such as polycrystalline or single-crystalline V_2O_5 nanorod arrays, $V_2O_5 \cdot n H_2O$ nanotube arrays, and Ni–$V_2O_5 \cdot n H_2O$ core-shell nanocable arrays. In analogy to vanadium oxides, nanostructured manganese oxides are synthesized with soft chemistry methods and different morphologies are produced including nanowires, nanotubes, nanobelts, mesoprous structures, and honeycomb-structured thin films. Morphology, structure, growth mechanisms, and electrochemical properties of these nanostructures have been discussed in this Review. All nanostructured electrodes exhibit significantly improved storage capacity and rate performance in comparison with thin-film electrodes. There are only a few studies on $LiFePO_4$ nanoparticles, and sub-micrometer-sized or micrometer-sized $LiFePO_4$ is more commonly reported. However, to increase the conductivity of this material, carbon or metallic coatings with thicknesses on the order of a few nanometers are deposited on the surface of $LiFePO_4$, mostly during the synthesis process. Such novel designs of nanostructured

ADVANCED MATERIALS

composites are generalized and applied to other oxides and conductive materials, including composites of carbon-oxide, polymer-oxide, metal-oxide, carbon-polymer, oxide-oxide or even metal-oxide-polymer.

In addition to all the benefits derived from the huge surface area, short distance for mass and charge transport, and freedom of volume change offered by nanostructured cathode materials, the benefits come with extra challenges. The huge surface area and nanometer dimensions render increased solubility of electrode materials in electrolyte solution; the increased chemical activities may also make the electrode materials more sensitive to impurities and contaminants. Application of a thin coating is an easy fix to bulk materials when the surface chemistry and physical properties need to be altered; however, a coating on nanostructured materials may not be so easy. A nanosized thin coating with conformal coverage on nanostructures, without unwanted deposition and aggregation, is a challenge. In this aspect, nanorod, nanotube, and nanocable arrays offer obvious advantages over nanoparticles. One-dimensional nanostructures suffer less increased solubility than nanoparticles, and it is easier to apply a conformal coating on them.

Applications of nanotechnology in energy storage are in the stage of research and development. For realization of wide industrial applications, further work is required to achieve controlled and large-scale synthesis of nanostructures, and to understand the mechanisms of lithium storage in nanomaterials and kinetic transport on the interface between electrode and electrolyte. The effects of nanostructures in battery performance are not only simple consequences of a reduction in size. Interfacial properties are subtle and critical, considering space-charge effects at the interface between nanosized electrode materials and charge transport between electrode and electrolyte. This challenges researchers worldwide to carry out systematic experimental studies and to develop predictive theoretical tools for a better fundamental understanding of the relationships between nanostructures and electrochemical characteristics of electrode materials.

Received: September 5, 2007
Published online: May 26, 2008

[1] *Advances in Lithium-Ion Batteries* (Eds: W. van Schalkwijk, B. Scrosati), Springer, Berlin **2002**.
[2] J. M. Tarascon, M. Armand, *Nature* **2001**, *414*, 359.
[3] G. Z. Cao, *Nanostructures and Nanomaterials, Synthesis, Properties and Applications*, Imperial College, London **2004**.
[4] A. Bachtold, P. Hadley, T. Nakanishi, C. Dekker, *Science* **2001**, *294*, 1317.
[5] R. Martel, T. Schmidt, H. R. Shea, T. Hertel, P. Avouris, *Appl. Phys. Lett.* **1998**, *73*, 2447.
[6] G. Zheng, W. Lu, S. Jin, C. M. Lieber, *Adv. Mater.* **2004**, *16*, 1890.
[7] Y. W. Heo, L. C. Tien, Y. Kwon, D. P. Norton, S. J. Pearton, B. S. Kang, F. Ren, *Appl. Phys. Lett.* **2004**, *85*, 2274.
[8] Y. Cui, Q. Wei, H. Park, C. M. Lieber, *Science* **2001**, *293*, 1289.
[9] A. Star, T. Han, V. Joshi, J. P. Gabriel, G. Grüner, *Adv. Mater.* **2004**, *16*, 2049.
[10] E. Comini, G. Faglia, G. Sberveglieri, Z. W. Pan, Z. L. Wang, *Appl. Phys. Lett.* **2002**, *81*, 1869.
[11] E. S. Snow, F. K. Perkins, E. J. Houser, S. C. Badescu, T. L. Reinecke, *Science* **2005**, *307*, 1942.
[12] H. J. Dai, J. H. Hafner, A. G. Rinzler, D. T. Golbert, R. E. Smalley, *Nature* **1996**, *384*, 147.
[13] Y. Zhang, K. Suenaga, C. Colliex, S. Iijima, *Science* **1998**, *281*, 973.
[14] J. C. Hulteen, C. R. Martin, *J. Mater. Chem.* **1997**, *7*, 1075.
[15] N. Pinna, U. Wild, J. Urban, R. Schlögl, *Adv. Mater.* **2003**, *15*, 329.
[16] M. Winter, R. J. Brodd, *Chem. Rev.* **2004**, *104*, 4245.
[17] D. O'Hare, *Inorganic Materials* (Eds: D.W. Bruce, D. O'Hare), Wiley, New York **1991**, p. 165.
[18] R. Schöllhorn, *Angew. Chem. Int. Ed. Engl.* **1980**, *19*, 983.
[19] R. Schöllhorn, *Chemical Physics of Intercalation*, NATO Series B, Vol. 172, Plenum, New York **1987**, p. 149.
[20] D. W. Murphy, S. A. Sunshine, S. M. Zahurak, *Chemical Physics of Intercalation*, NATO Series B, Vol. 172, Plenum, New York **1987**, p. 173.
[21] D. W. Murphy, P. A. Christian, F. J. DiSalvo, J. V. Waszczak, *Inorg. Chem.* **1985**, *24*, 1782.
[22] R. Clement, *J. Am. Chem. Soc.* **1981**, *103*, 6998.
[23] L. F. Nazar, A. J. Jacobson, *J. Chem. Soc. Chem. Commun.* **1986**, *570*.
[24] R. Schöllhorn, *Physics of Intercalation Compounds*, Springer, Berlin **1981**.
[25] A. S. Aricò, P. Bruce, B. Scrosati, J.-M. Tarascon, W. V. Schalkwijk, *Nat. Mater.* **2005**, *4*, 366.
[26] M. S. Whittingham, *Chem. Rev.* **2004**, *104*, 4271.
[27] M. S. Whittingham, Y. Song, S. Lutta, P. Y. Zavalij, N. A. Chernova, *J. Mater. Chem.* **2005**, *15*, 3362.
[28] J. N. Reimers, J. R. Dahn, *J. Electrochem. Soc.* **1992**, *139*, **2091**.
[29] P. N. Kumta, D. Gallet, A. Waghray, G. E. Blomgren, M. P. Setter, *J. Power Sources* **1998**, *72*, 91.
[30] T. Ohzuku, A. Ueda, N. Nagayama, Y. Iwakoshi, H. Komori, *Electrochim. Acta* **1993**, *38*, 1159.
[31] G. G. Amatucci, J. M. Tarascon, L. C. Klein, *J. Electrochem. Soc.* **1996**, *143*, 1114.
[32] T. Ohzuku, A. Ueda, *Solid State Ionics* **1994**, *69*, 201.
[33] T. Ohzuku, A. Ueda, N. Nagayama, *J. Electrochem. Soc.* **1993**, *140*, 1862.
[34] J. R. Dahn, U. von Sacken, C. A. Michal, *Solid State Ionics* **1990**, *44*, 87.
[35] A. Rougier, P. Gravereau, C. Delmas, *J. Electrochem. Soc.* **1996**, *143*, 1168.
[36] L. Abello, E. Husson, Y. R. Repelin, G. Lucazeau, *Spectrochim. Acta* **1983**, *39A*, 641.
[37] M. M. Thackeray, *J. Electrochem. Soc.* **1995**, *142*, 2558.
[38] B. Ammundesen, J. Paulsen, *Adv. Mater.* **2001**, *13*, 943.
[39] J. B. Goodenough, K. Mizuchima, *US Patent 4302518*, **1981**.
[40] P. S. Herle, B. Ellis, N. Coombs, L. F. Nazar, *Nat. Mater.* **2002**, *1*, 123.
[41] C. J. Curtis, J. Wang, D. L. Schulz, *J. Electrochem. Soc.* **2004**, *151*, A590.
[42] J. F. Whitacre, W. C. West, E. Brandon, B. V. Ratnakumar, *J. Electrochem. Soc.* **2001**, *148*, A1078.
[43] M. Kunduraci, G. G. Amatucci, *J. Electrochem. Soc.* **2006**, *153*, A1345.
[44] J. C. Arrebola, A. Caballero, M. Cruz, L. Hernán, J. Morales, E. R. Castellón, *Adv. Funct. Mater.* **2006**, *16*, **1904**.
[45] D. W. Murphy, P. A. Christian, F. J. DiSalvo, J. V. Waszczak, *Inorg. Chem.* **1979**, *18*, 2800.
[46] L. Abello, E. Husson, Y. R. Repelin, G. Lucazeau, *Spectrochim. Acta* **1983**, *39A*, 641.
[47] M. S. Whittingham, *J. Electrochem. Soc.* **1975**, *122*, 315.

[48] Y. Sakurai, S. Okada, J. Yamaki, T. Okada, *J. Power Sources* **1987**, *20*, 173.
[49] K. West, B. Zachau-Christiansen, M. J. L. Ostergard, T. Jacobsen, *J. Power Sources* **1987**, *20*, 165.
[50] K. West, B. Zachau-Christiansen, T. Jacobsen, S. Skaarup, *Electrochim. Acta* **1993**, *38*, 1215.
[51] K. Salloux, F. Chaput, H. P. Wong, B. Dunn, M. W. Breiter, *J. Electrochem. Soc.* **1995**, *142*, L191.
[52] V. Petkov, P. N. Trikalitis, E. S. Bozin, S. J. L. Billinge, T. Vogt, M. G. Kanatzidis, *J. Am. Chem. Soc.* **2002**, *124*, 10157.
[53] R. Nesper, M. E. Spahr, M. Niederberger, P. Bitterli, *Int. Patent Appl. PCT/CH97/00470,* **1997**.
[54] M. E. Spahr, P. Bitterli, R. Nesper, M. Müller, F. Krumeich, H.-U. Nissen, *Angew. Chem.* **1998**, *110*, 1339.
[55] M. E. Spahr, P. Bitterli, R. Nesper, M. Müller, F. Krumeich, H.-U. Nissen, *Angew. Chem. Int. Ed.* **1998**, *37*, 1263.
[56] F. Krumeich, H.-J. Muhr, M. Niederberger, F. Bieri, B. Schnyder, R. Nesper, *J. Am. Chem. Soc.* **1999**, *121*, 8324.
[57] H.-J. Muhr, F. Krumeich, U. P. Schòholzer, F. Bieri, M. Niederberger, L. J. Gauckler, R. Nesper, *Adv. Mater.* **2000**, *12*, 231.
[58] K. S. Pillai, F. Krumeich, H.-J. Muhr, M. Niederberger, R. Nesper, *Solid State Ionics* **2001**, *141-142,* 185.
[59] C. J. Patrissi, C. R. Martin, *J. Electrochem. Soc.* **1999**, *146*, 3176.
[60] N. Li, C. J. Patrissi, C. R. Martin, *J. Electrochem. Soc.* **2000**, *147*, 2044.
[61] C. R. Sides, C. R. Martin, *Adv. Mater.* **2005**, *17*, 125.
[62] K. Takahashi, S. J. Limmer, Y. Wang, G. Z. Cao, *J. Phys. Chem. B* **2004**, *108*, 9795.
[63] K. Takahashi, S. J. Limmer, Y. Wang, G. Z. Cao, *Jpn. J. Appl. Phys. Part 1* **2005**, *44*, 662.
[64] K. Takahashi, Y. Wang, G. Z. Cao, *Appl. Phys. Lett.* **2005**, *86*, 053102.
[65] A. van der Drift, *Philips Res. Rep.* **1968**, *22*, 267.
[66] R. L. Penn, J. F. Banfield, *Geochim. Cosmochim. Acta* **1999**, *63*, 1549.
[67] C. M. Chun, A. Navrotsky, I. A. Aksay, in *Proceedings of Microscopy and Microanalysis* (Eds: G. W. Bailey, M. H. Ellisman, R. A. Hennigar, N. J. Zaluzec), Jones and Begell, New York, NY **1995**, 188.
[68] Y. Wang, K. Takahashi, H. Shang, G. Z. Cao, *J. Phys. Chem. B* **2005**, *109*, 3085.
[69] K. Takahashi, Y. Wang, G. Z. Cao, *J. Phys. Chem. B* **2005**, *109*, 48.
[70] K. Lee, Y. Wang, G. Z. Cao, *J. Phys. Chem. B* **2005**, *109*, 16700.
[71] C. Navone, R. Baddour-Hadjean, J. P. Pereira-Ramos, R. Salot, *J. Electrochem. Soc.* **2005**, *152*, A1790.
[72] H. Yan, S. Sokolov, J. C. Lytle, A. Stein, F. Zhang, W. H. Smyrl, *J. Electrochem. Soc.* **2003**, *150*, A1102.
[73] N. S. Ergang, J. C. Lytle, K. T. Lee, S. M. Oh, W. H. Smyrl, A. Stein, *Adv. Mater.* **2006**, *18*, 1750.
[74] P. Liu, S. Lee, E. Tracy, Y. Yan, J. A. Turner, *Adv. Mater.* **2002**, *14*, 27.
[75] D. Pan, S. Zhang, Y. Chen, J. G. Hou, *J. Mater. Res.* **2002**, *17*, 1981.
[76] U. Schlecht, M. Knez, V. Duppel, L. Kienle, M. Burghard, *Appl. Phys. A* **2004**, *78*, 527.
[77] J. Liu, X. Wang, Q. Peng, Y. Li, *Adv. Mater.* **2005**, *17*, 764.
[78] X. K. Hu, D. K. Ma, J. B. Liang, S. L. Xiong, J. Y. Li, Y. T. Qian, *Chem. Lett.* **2007**, 560.
[79] G. Li, S. Pang, L. Jiang, Z. Guo, Z. Zhang, *J. Phys. Chem. B* **2006**, *110*, 9383.
[80] B. Li, Y. Xu, G. Rong, M. Jing, Y. Xie, *Nanotechnology* **2006**, *17*, 2560.
[81] X. Li, W. Li, H. Ma, J. Chen, *J. Electrochem. Soc.* **2007**, *154*, A39.
[82] S. T. Lutta, H. Dong, P. Y. Zavalij, M. S. Whittingham, *Mater. Res. Bull.* **2005**, *40*, 383.
[83] C. K. Chan, H. Peng, R. D. Tweten, K. Jarausch, X. F. Zhang, Y. Cui, *Nano Lett.* **2007**, *7*, 490.
[84] W. C. West, N. V. Myung, J. F. Whitacre, B. V. Ratnakumar, *J. Power Sources* **2004**, *126*, 203.
[85] M. S. Wu, P. C. J. Chiang, J. T. Lee, J. C. Lin, *J. Phys. Chem. B* **2005**, *109*, 23279.
[86] F. Y. Cheng, J. Z. Zhao, W. E. Song, C. S. Li, H. Ma, J. Chen, P. W. Shen, *Inorg. Chem.* **2006**, *45*, **2038**.
[87] W. H. Ho, S. K. Yen, *J. Electrochem. Soc.* **2005**, *152*, A506.
[88] F. Jiao, P. T. Bruce, *Adv. Mater.* **2007**, *19*, 657.
[89] R. Ma, Y. Bando, L. Zhang, T. Sasaki, *Adv. Mater.* **2004**, *16*, 918.
[90] J. Kim, Manthiram, *Nature* **1997**, *390*, 265.
[91] D. Im, A. Manthiram, *J. Electrochem. Soc.* **2002**, *149*, A1001.
[92] J. Yang, J. J. Xu, *J. Power Sources* **2003**, *122*, 181.
[93] J. Kim, M. Noh, J. Cho, H. Kim, K. Kim, *J. Electrochem. Soc.* **2005**, *152*, A1142.
[94] J. Cho, B. Kim, J. Lee, Y. Kim, B. Park, *J. Electrochem. Soc.* **2005**, *152*, A32.
[95] B. Kim, C. Kim, T. Kim, D. Ahn, B. Park, *J. Electrochem. Soc.* **2006**, *153*, A1773.
[96] Y. J. Kim, J. Cho, T.-J. Kim, B. Park, *J. Electrochem. Soc.* **2003**, *150*, A1723.
[97] L. Lui, Z. Wang, H. Li, L. Chen, X. Huang, *Solid State Ionics* **2002**, *152-153, 341.*
[98] J. Cho, C.-S. Kim, S.-I. Yoo, *Electrochem. Solid-State Lett.* **2000**, *3*, 362.
[99] Z. Wang, X. Huang, L. Chen, *J. Electrochem. Soc.* **2003**, *150*, A199.
[100] T. Fang, J. Duh, S. Sheen, *J. Electrochem. Soc.* **2005**, *152*, A1701.
[101] T. Tang, J. Duh, S. R. Sheen, *J. Electrochem. Soc.* **2005**, *152*, A1701.
[102] K. Y. Chung, W. Yoon, J. McBreen, X. Yang, S. H. Oh, H. C. Shin, W. I. Cho, B. W. Cho, *J. Electrochem. Soc.* **2006**, *153*, A2152.
[103] H. Miyashiro, A. Yamanaka, M. Tabuchi, S. Seki, M. Nakayama, Y. Ohno, Y. Kobayashi, Y. Mita, A. Usami, M. Wakihara, *J. Electrochem. Soc.* **2006**, *153*, A348.
[104] N. Ohta, K. Takada, L. Zhang, R. Ma, M. Osada, T. Sasaki, *Adv. Mater.* **2006**, *18*, 2226.
[105] Y. Sun, K. Hong, J. Prakash, *J. Electrochem. Soc.* **2003**, *150*, A970.
[106] J. Han, S. Myung, Y. Sun, *J. Electrochem. Soc.* **2006**, *153*, A1290.
[107] M. M. Thackeray, C. S. Johnson, J. S. Kim, K. C. Lauzze, J. T. Vaughey, N. Dietz, D. Abraham, S. A. Hackney, W. Zeltner, M. A. Anderson, *Electrochem. Commun.* **2003**, *5*, 752.
[108] J. S. Kim, C. S. Johnson, J. T. Vaughey, S. A. Hackney, K. A. Walz, W. A. Zeltner, M. A. Anderson, M. M. Thackeray, *J. Electrochem. Soc.* **2004**, *151*, A1755.
[109] S. Franger, F. L. Cras, C. Bourbon, H. Rouault, *Electrochem. Solid-State Lett.* **2002**, *5*, A231.
[110] P. P. Prosini, M. Lisi, D. Zane, M. Pasquali, *Solid State Ionics* **2002**, *148*, 45.
[111] D. Y. W. Yu, C. Fietzek, W. Weydanz, K. Donoue, T. Inoue, H. Kurokawa, S. Fujitani, *J. Electrochem. Soc.* **2007**, *154*, A253.
[112] S.-Y. Chung, J. T. Bloking, Y.-M. Chiang, *Nat. Mater.* **2002**, *1*, 123.
[113] S. Yang, Y. Song, K. Ngala, P. Y. Zavalij, M. S. Whittingham, *J. Power Sources* **2003**, *119*, 239.
[114] N. Ravet, J. B. Goodenough, S. Besner, M. Simoneau, P. Hovington, M. Armand, *Electrochem. Soc. Abstr.* **1999**, *99-2*, 172.
[115] N. Ravet, S. Besner, M. Simoneau, A. Vallée, M. Armand, J.-F. Magnan, *Eur. Patent 1049182A2,* **2000**.
[116] S. Yang, P. Y. Zavalij, M. S. Whittingham, *Electrochem. Commun.* **2001**, *3*, 505.
[117] A. D. Spong, G. Vitins, J. R. Owen, *J. Electrochem. Soc.* **2005**, *152*, A2376.
[118] T. Nakamura, Y. Miwa, M. Tabuchi, Y. Yamada, *J. Electrochem. Soc.* **2006**, *153*, A1108.
[119] M. Gaberscek, R. Dominko, M. Bele, M. Remskar, D. Hanzel, J. Jamnik, *Solid State Ionics* **2005**, *176*, 1801.
[120] J. D. Wilcox, M. M. Doeff, M. Marcinek, R. Kostecki, *J. Electrochem. Soc.* **2007**, *154*, A389.

ADVANCED MATERIALS

[121] R. Dominko, J. M. Goupil, M. Bele, M. Gaberscek, M. Remskar, D. Hanzel, J. Jamnik, *J. Electrochem. Soc.* **2005**, *152*, A858.
[122] F. Croce, A. D. Epifanio, J. Hassoun, A. Deptula, T. Olczac, B. Scrosati, *Electrochem. Solid-State Lett.* **2002**, *5*, A47.
[123] Y.-H. Rho, L. F. Nazar, L. Perry, D. Ryan, *J. Electrochem. Soc.* **2007**, *154*, A283.
[124] H.-M. Xie, R.-S. Wang, J.-R. Ying, L.-Y. Zhang, A. F. Jalbout, H.-Y. Yu, G.-L. Yang, X.-M. Pan, Z.-M. Su, *Adv. Mater.* **2006**, *18*, 2609.
[125] Y.-H. Huang, K.-S. Park, J. B. Goodenough, *J. Electrochem. Soc.* **2006**, *153*, A2282.
[126] Y.-S. Hu, Y.-G. Guo, R. Dominko, M. Gaberscek, J. Jamnik, *Adv. Mater.* **2007**, *19*, 1963.
[127] H. Huang, S.-C. Yin, L. F. Nazar, *Electrochem. Solid-State Lett.* **2001**, *4*, A170.
[128] K.-F. Hsu, S.-Y. Tsay, B.-J. Hwang, *J. Mater. Chem.* **2004**, *14*, 2690.
[129] K. Padhi, K. S. Nanjundaswamy, J. B. Goodenough, *J. Electrochem. Soc.* **1997**, *144*, 1188.
[130] J. M. Tarascon, C. Delacourt, A. S. Prakash, M. Morcrette, M. S. Hegde, C. Wurm, C. Masquelier, *Dalton Trans.* **2004**, 2988.
[131] M. Koltypin, V. Pol, A. Gedanken, D. Aurbach, *J. Electrochem. Soc.* **2007**, *154*, A605.
[132] J. S. Sakamoto, B. Dunn, *J. Electrochem. Soc.* **2002**, *149*, A26.
[133] D. Dubarry, J. Gaubicher, P. Moreau, D. Guyomard, *J. Electrochem. Soc.* **2006**, *153*, A295.
[134] X. Huang, H. Yue, A. Attia, Y. Yang, *J. Electrochem. Soc.* **2007**, *154*, A26.
[135] H. Kawaoka, M. Hibino, H. Zhou, I. Honma, *J. Electrochem. Soc.* **2005**, *152*, A1217.
[136] J. Yang, J. J. Xu, *J. Electrochem. Soc.* **2006**, *153*, A716.
[137] H. Huang, S.-C. Yin, T. Kerr, N. Taylor, L. F. Nazar, *Adv. Mater.* **2002**, *14*, 1525.
[138] M. Ferreira, V. Zucolotto, F. Huguenin, R. M. Torresi, O. N. Oliveira, Jr., *J. Nanosci. Nanotechnol.* **2002**, *2*, 29.
[139] F. Huguenin, D. S. dos Santos, Jr., A. Bassi, F. C. Nart, O. N. Oliveira, Jr., *Adv. Funct. Mater.* **2004**, *14*, 985.
[140] E. A. Ponzio, T. M. Benedetti, R. M. Torresi, *Electrochim. Acta* **2007**, *52*, 4419.
[141] C. V. S. Reddy, W. Jin, Q.-Y. Zhu, W. Chen, R. R. Kalluru, *Eur. Phys. J. Appl. Phys.* **2007**, *10*, 31.
[142] E. A. Olivetti, J. H. Kim, D. R. Sadoway, A. Asatekin, A. M. Mayes, *Chem. Mater.* **2006**, *18*, 2828.
[143] D. Guy, B. Lestriez, D. Guyomard, *Adv. Mater.* **2004**, *16*, 553.
[144] N. Peter, M. Klaus, K. S. V. Santhannam, H. Otto, *Chem. Rev.* **1997**, *97*, 207.
[145] J. Wang, J. Yang, J. Xie, N. Xu, *Adv. Mater.* **2002**, *14*, 963.
[146] J. Wang, J. Yang, C. Wan, K. De, J. Xie, N. Xu, *Adv. Funct. Mater.* **2003**, *13*, 487.
[147] P. Novák, K. Müller, K. S. V. Santhanan, O. Haas, *Chem. Rev.* **1999**, *99*, 207.
[148] K.-S. Park, S. B. Schougaard, J. B. Goodenough, *Adv. Mater.* **2007**, *19*, 848.
[149] Y. Wang, K. Lee, H. Shang, B. Wiley, Y. Xia, G. Cao, *Phys. Status Solidi A* **2005**, *202*, R79.
[150] J. S. Wook, S.-M. Lee, *J. Electrochem. Soc.* **2007**, *154*, A22.
[151] Y. Li, T. Kunitake, Y. Aoki, *Chem. Mater.* **2007**, *19*, 575.
[152] N. Imachi, Y. Takano, H. Fujimoto, Y. Kida, S. Fujitani, *J. Electrochem. Soc.* **2007**, *154*, A412.
[153] S. R. Sivakkumar, D. R. MacFarlane, M. Forsyth, D.-W. Kim, *J. Electrochem. Soc.* **2007**, *154*, A834.